Constitutive activation of WASp in X-linked neutropenia renders neutrophils hyperactive

Marton Keszei[1,*], Julien Record[1], Joanna S. Kritikou[1], Hannah Wurzer[1], Chiara Geyer[1], Meike Thiemann[1], Paul Drescher[1], Hanna Brauner[1], Laura Köcher[1], Jaime James[1], Minghui He[1], Marisa A.P. Baptista[1], Carin I.M. Dahlberg[1], Amlan Biswas[2], Sonia Lain[1], David P. Lane[1], Wenxia Song[3], Katrin Pütsep[1], Peter Vandenberghe[4], Scott B. Snapper[2], Lisa S. Westerberg[1,*]

[1] Department of Microbiology Tumor and Cell biology, Karolinska Institutet, Stockholm 171 77, Sweden

[2] Gastroenterology Division, Children's Hospital, Harvard Medical School, Boston, MA 02115, USA

[3] Department of Cell Biology & Molecular Genetics, University of Maryland, College Park, MD 207423, USA

[4] Center for Human Genetics, KU Leuven and Hematology/Internal Medicine, University Hospitals Leuven, Leuven , Belgium

[*]Corresponding Authors:

Lisa S. Westerberg, Ph.D., Karolinska Institutet, Department of Microbiology, Tumor and Cell biology, Biomedicum, Solnavägen 9, SE-171 65 Stockholm, Sweden, Phone: +46 8 52486833, Fax: +46 8 52487150, Email: Lisa.Westerberg@ki.se

Marton Keszei, Ph.D., Karolinska Institutet, Department of Microbiology, Tumor and Cell biology, Biomedicum, Solnavägen 9, SE-171 65 Stockholm, Sweden, Phone: +46 8 52486833, Fax: +46 8 52487150, Email: Marton.Keszei@ki.se

Number of words: 11221

Abstract: 200

Number of figures: 8 figures + 7 supplementary Figures

Number of tables: 0

Running title: WASp activity regulates neutrophil function

Keywords: Neutrophils, WASp, X-linked neutropenia, Wiskott-Aldrich syndrome protein, migration, adhesion

Abbreviations: ANC, absolute neutrophil count; Btk, Bruton's tyrosine kinase; fMLP, N-formyl-met-leu-phe; PI3K, phosphoinositide 3-kinase; PIP2, phosphatidylinositol 4,5-bisphosphate; GFP, green fluorescent protein; PMA, phorbol myristate acetate; ROS, reactive oxygen species; SCN, severe congenital neutropenia; WASp, Wiskott-Aldrich syndrome protein; WKO, WASp knockout; XLN; X-linked neutropenia; DFP, diisopropyl fluorophosphate

ABSTRACT

Congenital neutropenia is characterized by low absolute neutrophil number in blood leading to recurrent bacterial infections and patients often require life-long G-CSF support. X-linked neutropenia (XLN) is caused by gain-of-function mutations in the actin regulator Wiskott-Aldrich syndrome protein (WASp). To understand the pathophysiology in XLN and the role of WASp in neutrophils, we here examined XLN patients and two novel XLN mouse models. XLN patients had reduced myelopoiesis and extremely low blood neutrophil number. However, their neutrophils had a hyperactive phenotype and were present in normal number in XLN patient saliva. Murine XLN neutrophils were hyper-activated with increased actin dynamics and migration into tissues. We provide molecular evidence for that the hyperactivity of XLN neutrophils is caused by WASp in a constitutively open conformation due to contingent phosphorylation of the critical tyrosine-293 and plasma membrane localization. This renders WASp activity less dependent on regulation by phosphoinositide-3-kinase. Our data shows that the amplitude of WASp activity inside a cell could be enhanced by cell surface receptor signalling even in the context where WASp is already in an active conformation. Moreover, this data categorizes XLN as an atypical congenital neutropenia where constitutive activation of WASp in tissue neutrophils compensates for reduced myelopoiesis.

INTRODUCTION

Severe congenital neutropenia (SCN) is characterized by low absolute neutrophil count in blood that leads to life-threating infections and requires administration of granulocyte colony-stimulating factor (G-CSF) to stimulate the number of circulating neutrophils (1-3). Mutations in ELA2/ELANE, HCLS1-associated protein X (HAX)1, adenylate kinase (AK)2, glucose-6-phosphate complex (G6PC)3, and Jagunal homolog 1 (JAGN1) cause SCN due to premature apoptosis of myeloid progenitor cells. Other genetic defects are associated with neutrophil dysfunction, such as mutations in the CYBB gene causing X-linked chronic granulomatous disease (CGD) where NADPH oxidase fails to produce reactive oxygen species (ROS) and neutrophils are defective in killing bacteria (4) or mutations in the beta 2 integrin family that cause leukocyte adhesion deficiency type I (LAD-I) characterized by lack of neutrophil transmigration through the activated endothelium (5).

The dynamics of the actin cytoskeleton is a critical feature of rapidly moving and acting cells such as neutrophils. Local inflammation activates the endothelium that upregulates P- and E-selectins that binds to glycosylated ligands on neutrophils such as sialyl-LewisX and P-selectin glycoprotein ligand 1 (PSGL1) (6, 7). This allows fast moving neutrophils in blood vessels to get tethered to the endothelial surface and start rolling along the vessel wall. Chemoattractants, such as formyl-peptides and CXCL1 (IL-8), activate β2 integrin molecules on neutrophils that bind to intercellular adhesion molecule (ICAM)-1 and -2 on the activated endothelium and mediate firm adhesion between neutrophils and the endothelium (6, 7). Neutrophil spreading is an essential step between crawling and arrest in search for permissive sites to migrate through the endothelium into the tissue (8). In tissues, neutrophils use an amoeboid-type of migration characterized by intracellular polarization of the small Rho GTPases Rac2, Cdc42, and RhoA that gives rise to a leading edge lamellipodia in the front and a trailing uropod at the rear of the migrating cell. Failure to regulate the actin cytoskeleton impair neutrophil number and function, as it is demonstrated by mutations in the genes encoding for non-muscular β-actin, the actin sensor megakaryoblastic leukemia 1 (MKL1), and the actin regulator Wiskott-Aldrich syndrome protein (WASp) (9-17).

The gene encoding WASp is uniquely expressed in hematopoietic cells and highly expressed during neutrophil maturation (Immgen.org). WASp is critically dependent on its structural conformation for activity and is predicted to reside in an inactive form in the cytoplasm

caused by an intramolecular interaction between the GTPase binding domain (GBD) and the C-terminal verprolin-cofilin-acidic (VCA) domain (18, 19). WASp binding to the small GTPase Cdc42 and phosphatidylinositol 4,5-bisphosphate (PIP2) releases the auto-inhibition and exposes the VCA domain to the Arp2/3 complex that induces actin polymerization (18-20). The open conformation exposes the tyrosine Y291 (Y293 in mouse) in the GBD that when phosphorylated increases the basal activity of WASp towards the Arp2/3 complex, even upon dissociation from Cdc42 (21). In addition, phosphorylated WASp can be activated by Src family kinases and Tec family kinases including Bruton's tyrosine kinase (Btk) (21-23).

The importance of WASp in hematopoietic cells is illustrated by two primary immunodeficiency syndromes; Wiskott-Aldrich syndrome (WAS) and X-linked neutropenia (XLN). WAS patients harbour loss-of-function mutations in WASp and suffer from eczema, microthrombocytopenia, and severe immunodeficiency, while XLN patients with gain-of-function mutations in the WASp GBD domain (L270P, S272P, or I294T) exhibit severe neutropenia and monocytopenia. XLN is considered a SCN, however, a puzzling clinical observation is that despite extremely low number of circulating neutrophils (less than 0.3 x 10^9/L), XLN patients are generally not at high risk of infections, and therefore do not require permanent G-CSF support (15). The lack of correlation between the circulating neutrophil number and rate of infections in XLN patients indicates that XLN should be distinguished from classical SCNs and requires more mechanistic understanding of the disease.

To understand how the activity of WASp needs to be regulated for normal neutrophil hematopoiesis, trafficking and function, we here combined investigation of neutrophils from two XLN patients carrying the WASp L270P mutations with analysis of two novel mouse models harbouring the corresponding human XLN mutations WASp L272P and WASp I296T. WASp L270P patients had defective myelopoiesis, which would predict low peripheral neutrophil number, however, patients had normal neutrophil number in the saliva, suggesting a compensatory response for decreased bone marrow myeloid output. We found that neutrophils in WASp L272P and WASp I296T XLN mice were hyperactive in vitro and in vivo. We define that XLN is caused by hyper-phosphorylated WASp that is constitutively recruited to the plasma membrane to induce actin dynamics. In this study, we provide mechanistic insight into the clinical disease in XLN patients by showing that despite decreased myelopoiesis, neutrophils are functional in tissues due to increased WASp activity, needed in all steps of neutrophil functionality.

RESULTS

Low number of neutrophils in circulation and impaired hematopoiesis in XLN patients

To examine neutrophil granulocytes of WASp XLN patients, we collected blood from a previously described pedigree (16) including two brothers with the WASp L270P mutation (X1 and X2), their asymptomatic carrier mother (M), the sister with unknown carrier status (S), and from two healthy unrelated males serving as controls (C1 and C2). The numbers of granulocytes and monocytes and their ratios in the blood of X1 and X2 patients were dramatically decreased when compared to M, S, C1, and C2 (**Figure 1A-D** and **Supplemental Figure 1A-B**). Consequently, the percentage of lymphocytes in the blood of XLN patients was high (**Figure 1A**) but the absolute lymphocyte number was normal (**Supplemental Figure 1C**). Granulocyte populations were divided into $CD15^{hi}CD16^{hi}$ and $CD15^{lo}CD16^{lo}$ cells, corresponding to neutrophils and eosinophils in control samples, respectively (24) (**Figure 1B**). The numbers and ratio of neutrophils was severely reduced in X1 and X2 patients and XLN neutrophils had low expression of CD16 (**Figure 1B**), indicating immaturity of granulocytes (24). Although the relative ratio of eosinophils to neutrophils was increased in XLN patients, the absolute eosinophil number was similar to controls (**Supplemental Figure 1D**). Gating on the neutrophil population, this population could be divided into $CD16^{hi}CD11b^{hi}$ and $CD16^{lo}CD11b^{hi}$ cells, corresponding to mature neutrophils / band cells and metamyelocytes, respectively (**Supplemental Figure 1A**). The control samples contained mostly mature neutrophils / band cells, while X1 and X2 samples contained a large proportion of metamyelocytes with reduced CD16 expression (**Supplemental Figure 1A**).

Human cathelicidin, hCAP18, is produced during myelopoiesis at the myelocyte stage of maturation. The disappearance of hCAP18 from serum is an indicator of myeloid maturation arrest in the bone marrow as seen in SCN1, SCN3, and various bone-marrow failure disorders (25, 26). We found that compared to C1, C2, and S, hCAP18 levels were reduced in X1 and M serum samples, and was below detection limit in the X2 sample (**Figure 1E-F and Supplemental Figure 1E**). Healthy individuals have >40% hCAP18 in serum (25, 26) and the carrier mother (M) was just below the normal range (**Figure 1E** and **Supplemental**

Figure 1E). This result indicates a perturbed bone-marrow myeloid maturation in the XLN patients.

We enriched $CD34^+$ stem cells and progenitor cells from blood of XLN patients and healthy donors (**Figure 1G-H**). Upon culturing $CD34^+$ cells *in vitro* with IL-3, SCF, and G-CSF, the proportion of $CD15^+CD11b^+$ neutrophils was lower in patients than in healthy controls (**Figure 1H**). The carrier mother showed an intermediate phenotype (**Figure 1H)**.

Since XLN patient neutrophils showed altered expression of surface molecules, we next examined granulocyte morphology by standard density gradient centrifugation and microscopy of blood cells (27). Corresponding to their reduced ratio by flow cytometry, XLN samples yielded a 24-fold lower granulocytes/ml blood when compared to controls (C1, C2, M, and S). While the granulocyte-enriched preparation contained over 80% neutrophils in control samples, X1 and X2 preparations contained approximately equal proportion of non-granulocytes, eosinophils and neutrophil-related cells (**Supplemental Figure 1F-G**), indicating that in the absence of neutrophils, non-granulocyte and eosinophil were enriched in the preparation. Manual counting of cell populations on cytospin images showed similar ratios **(Supplemental Figure 1H-I)** as observed with flow cytometry.

Taken together, we observed that XLN patients have reduced number of neutrophils in peripheral blood and defective myelopoiesis.

XLN neutrophils are hyper-activated in blood and they are present at normal number in saliva

To examine the ultrastructural features of XLN neutrophils, we used transmission electron microscopy. When compared to C1 and C2 controls, X1 and X2 neutrophils showed an apparent reduction of electron-dense granules and had a more activated de-granulated morphology (**Figure 2A and Supplemental Figure 2A**).

Further examination of neutrophils revealed a 4-6 fold higher expression of Gp91phox, a marker of activation, on XLN neutrophils compared to controls before (**Figure 2B**) and after (**Figure 2C**) stimulation using phorbol myristate acetate (PMA). This indicates that neutrophils were spontaneously activated in patients.

The reduced peripheral blood neutrophil number in SCN patients is often associated with severe periodontitis and gingivitis (1). However, no periodontal disease has been reported in XLN patients. We collected saliva samples from WASp L270P patients X1 and X2, the carrier mother (M), and two healthy controls (C2 and C3) to examine neutrophils in saliva. Using imaging flow cytometer, we combined analysis of surface CD15 and CD45 staining and irregular nuclear morphology to identify neutrophils (**Figure 2D**). We found comparable numbers of neutrophils in control (C2, C3, M) and patient (X1, X2) samples (**Figure 2D**). When examined by toluidine blue staining and electron microscopy, both control and XLN samples contained several cells with multi-lobular nucleus and granular (partially degranulated) cytoplasm. (**Supplemental Figure 2B-C**). The presence of neutrophils in saliva suggests that XLN patient neutrophils have capacity to migrate to the gingival tissues thus protecting the oral site from periodontal diseases.

Murine WASp XLN is spontaneously phosphorylated and induces increased actin polymerization

To investigate how XLN mutations in WASp would impact on neutrophil trafficking and function, we generated two new mouse models harbouring the WASp L272P and the WASp I296T mutations (**Figure 3A**). The murine WASp L272P and I296T mutations correspond to human XLN mutations L270P and I294T and are part of the WASp GBD domain with 100% amino acid identity in mice and humans. The WASp L272P and WASp I296T mice had normal neutrophil counts in bone marrow, blood, and spleen when compared to littermate WT controls (**Supplemental Figure 3A-C**). Analysis of 1-2 years old mice (**Supplemental Figure 3D-E**) and of mice treated with G-CSF to stimulate myelopoiesis (**Supplemental Figure 3F-H**) showed similar neutrophil counts in WASp L272P, WASp I296T, and WT mice. As predicted by the auto-inhibited regulation of WASp (16, 18), neutrophil WASp L272P and WASp I296T were prone to degradation by neutrophil serine proteases *in vitro* when compared to WT WASp (**Figure 3B-C and Supplemental Figure 3I-J**). WASp L272P and WASp I296T were spontaneously phosphorylated at Y293, while WT WASp showed only a weak phosphorylation signal (**Figure 3D and Supplemental Figure 3K-L**). Despite protease inhibitor treatment, Y293-phosphorylated proteolytic fragments were detected in the XLN samples (**Supplemental Figure 3K-L**). WASp L272P and WASp I296T neutrophils had increased F-actin content compared to WT neutrophils as assessed by flow cytometry (**Figure 3E**). To analyse the distribution of cellular F-actin, we used confocal microscopy and found increased F-actin in both the cortex and cytoplasm of XLN neutrophils (**Figure 3F**).

Light microscopy and transmission electron microscopy analysis showed that bone marrow neutrophils from WASp L272P and WASp I296T mice had normal morphology (**Supplemental Figure 3M-O**). To study surface topography, bone marrow neutrophils were examined using scanning electron microscopy. WASp L272P and WASp I296T neutrophils had an increased proportion of cells with highly ruffled surfaces when compared to WT neutrophils (**Figure 3G**). These data suggest that WASp L272P and WASp I296T exist in an open conformation that is spontaneously phosphorylated in the absence of stimuli. Moreover, WASp L272P and WASp I296T induce increased polymerized actin associated with altered surface topography of neutrophils.

Increased migration of WASp XLN neutrophils to the spleen and to the site of inflammation

To test the functional consequence of WASp XLN mutation on neutrophil migration, we injected *S. aureus* into mice by intradermal and intraperitoneal injection and quantified infiltrated neutrophils at the injection sites. WASp L272P and WASp I296T mice had increased number of infiltrating neutrophils when compared to WT mice (**Figure 4A-B**). To address the competitive fitness of WASp L272P and WASp I296T neutrophils side by side, we used mixed bone marrow chimeras. A mix of congenic $CD45.1^+$ WT and $CD45.2^+$ mutant bone marrow cells were injected into lethally irradiated hosts and analysed 8-10 weeks post transfer. In the blood, WT, WASp L272P, and WASp I296T neutrophils showed similar ratio of cells when compared to the injected ratio of cells (**Figure 4C**). In contrast, WASp L272P and WASp I296T neutrophils showed a 2-fold competitive advantage over WT neutrophils in the bone marrow, spleen, and in peritoneum upon thioglycollate-induced peritonitis (**Figure 4C**), suggesting that WASp XLN neutrophils accumulate in tissues.

We next examined the possibility that WASp L272P or WASp I296T neutrophils migrated more rapidly from the blood into tissues. We used a competitive setting where a mix of bone marrow neutrophils expressing CD45.1 (WT) or CD45.2 (mutant) were injected intravenously into WT [CD45.1xCD45.2]F1 recipient mice. We applied the air pouch model to examine neutrophil extravasation and accumulation into an empty pocket of the skin. To attract neutrophils to extravasate through the endothelium, fMLP and TNFα were injected into the air pouch (**Figure 4D**). When compared to WT neutrophils, WASp L272P and WASp I296T neutrophils showed competitive advantage in homing into the spleen and the air pouch (**Figure 4D**). In contrast, WASp KO neutrophils had selective disadvantage in homing into

the spleen and the air pouch (**Figure 4D**). Together, this data suggests that WASp L272P and WASp I296T neutrophils migrated more rapidly from the blood and accumulated in the tissues.

Increased actin dynamics, spreading, and motility of WASp XLN neutrophils

WASp XLN neutrophils showed elevated total F-actin and WASp Y293 phosphorylation under static conditions. Neutrophil extravasation into tissues depends on coordinated changes in adhesion and migration. (7). This process is synchronised by actin dynamics to form adhesive structures by clustering of integrins such as CD11b, by forming vinculin containing podosomes, and by leading edge lamellipodia formation with rapid actin polymerization and depolymerisation. Wildtype and WASp L272P and WASp I296T neutrophils formed CD11b clusters and podosomes on fibrinogen coated surfaces (**Supplemental Figure 4A, D, E).** The lamellipodia of WASp L272P and WASp I296T neutrophils covered less area when compared to wildtype neutrophils (**Supplemental Figure 4F)** and podosome number in WASp L272P, but not in WASp I296T, neutrophils was decreased (**Supplemental Figure 4G)**. We next examined if the increased cortical F-actin in XLN WASp neutrophils would lead to more dynamic changes in cell shape and adhesion. To evaluate actin polymerization in live cells, we crossed WT, WASp L272P, and WASp I296T mice with Lifeact-EGFP transgenic mice that express a fluorescently tagged peptide with high affinity to F-actin (28). Cellular morphology of neutrophils from WASp L272P x Lifeact-EGFP and WASp I296T x Lifeact-EGFP mice was monitored with an imaging flow cytometer. Upon activation with phorbol myristate acetate (PMA) or N-formyl-met-leu-phe (fMLP), we found that neutrophils lost their circular shape and acquired an irregular shape (**Figure 5A**). When compared to WT x Lifeact-EGFP cells upon fMLP activation, WASp L272P x Lifeact-GFP and WASp I296T x Lifeact-EGFP neutrophils showed a higher proportion of cells with irregular shape (**Figure 5A**).

To examine if increased actin dynamics corresponded to increased WASp activation, we examined WASp Y293 phosphorylation by flow cytometry. The chemoattractant CXCL1 is produced by the activated endothelium to recruit neutrophils to the site of inflammation. When neutrophils were activated with CXCL1, WT neutrophils had a rapid transient phosphorylation of WASp Y293, while the WASp XLN neutrophils showed higher amplitude of phosphorylation that remained high during the four minutes monitored (**Figure 5B**). This

was associated with higher amplitude of actin polymerization in CXCL1 stimulated WASp XLN neutrophils when compared to WT neutrophils (**Figure 5C**).

Integrin mediated firm adhesion in postcapillary venules is actin mediated and dependent on WASp activity as determined in WASp knockout neutrophils (29). To model neutrophil adhesion in blood vessels, we placed neutrophils into plastic flow chambers coated with recombinant P-selectin, ICAM-1, and CXCL1 molecules. Under steady 2 dyn/cm^2 flow rate, WT neutrophils rolled on the substratum, arrested, and spread (**Figure 5D**). To test the hypothesis that increased *in vivo* migration was caused by increased integrin mediated attachment, we compared the release rate of arrested cells and spread cells of WT and WASp XLN neutrophils under increasing shear stress by flow rate. WASp L272P and WASp I296T neutrophils had similar rate of release when compared to WT neutrophils (**Figure 5E).** However, the percentage of spread cells among all adherent cells (arrested and spread) was higher in WASp L272P and WASp I296T neutrophils (**Figure 5F**), showing increased adhesion of WASp XLN neutrophils under shear stress. Analysis of random motility of spread cells revealed that WASp XLN neutrophils showed significantly higher random movement measured as displacement from the point of origin (**Figure 5G-H**). Together, this suggests that XLN neutrophils have a dynamic actin cytoskeleton leading to increased spreading and increased movement of spread cells.

Increased membrane translocation and Btk dependent phosphorylation of WASp in XLN neutrophils

We next examined if increased actin dynamics and adhesion under flow would correspond to increased migratory response of WASp XLN neutrophils. To test this possibility, we examined neutrophil migration *in vitro* towards the neutrophil chemoattractants C5a, N-formyl-met-leu-phe (fMLP), and CXCL1. WASp L272P and WASp I296T neutrophils showed increased migratory response to C5a, fMLP, and CXCL1 when compared to WT neutrophils (**Figure 6A-C**). To determine the mechanism of increased XLN neutrophil migration, we mixed WT (CD45.1) and WASp I296T (CD45.2) neutrophils and compared their migration rate towards C5a or CXCL1 with or without pre-treating the cells with various inhibitors of intracellular signalling (**Figure 6D**). Inhibitors that targeted the actin cytoskeleton, Src kinases, or Cdc42 affected the migration of WT and WASp I296T neutrophils similarly (**Figure 6E**). In contrast, treating neutrophils with the phosphatidylinositol 3-kinase (PI3K) inhibitor wortmannin gave WASp I296T neutrophils

migratory advantage over WT neutrophils (**Figure 6E**). Importantly, also low concentration of wortmannin gave migration advantage to WASp L272P and WASp I296T neutrophils (**Supplemental Figure 5A**).

Inhibition of PI3K by wortmannin affects the production and distribution of phosphatidylinositol derivatives in the plasma membrane. From biochemical studies, WASp may interact directly with one of these membrane derivatives, phosphatidylinositol 4,5-bisphosphate (PIP2), via the WASp pleckstrin homology domain (19). To examine if WASp XLN mutations affected plasma membrane localization of WASp, we used imaging flow cytometry and examined WASp localization in neutrophils. Upon CXCL1 activation, WASp was recruited from the cytoplasm to the plasma membrane in WT neutrophils (**Figure 6F, Supplemental Figure 5B**). WASp membrane translocation was inhibited by wortmannin, indicating that this process is PI3K dependent (**Figure 6F**). WASp L272P and WASp I296T were constitutively located proximal to the plasma membrane, even in the absence of CXCL1 stimulation (**Figure 6F, Supplemental Figure 5B**).

WASp XLN neutrophils were less sensitive to inhibition of PI3K in the transwell competitive assay and exhibited increased adhesion under flow which is a PI3K dependent process (**Supplemental Figure 5C**). This effect was not due to increased PI3K signalling in WASp L272P and WASp I296T neutrophils, since phosphorylation of AKT, a main target of PI3K, was similar in unstimulated and stimulated WT and WASp XLN neutrophils (**Supplemental Figure 5D-E**). To evaluate if WASp activation depends on PI3K induced signalling, we examined if pharmacological inhibition of PI3K and also Src kinases would inhibit the spontaneous Y293 phosphorylation of WASp XLN. High concentration of wortmannin or Src1 inhibitors did not reduce WASp phosphorylation in WASp L272P neutrophils (**Figure 6G, Supplemental Figure 5F**). Based on studies of macrophages and neutrophils, Btk has been suggested to phosphorylate WASp (30, 31). The Btk inhibitor Ibrutinib effectively reduced the spontaneous phosphorylation of Y293 in WASp L272P (**Figure 6H, Supplemental Figure 5G**). To examine if Ibrutinib could affect sustained phosphorylation of WASp XLN, we examined pWASp Y293 upon CXCL1 stimulation by flow cytometry. Ibrutinib treatment lowered the sustained hyperphosphorylation of WASp XLN (**Figure 6I**). To examine the functional consequence of Ibrutinib treatment of WASp XLN neutrophils, we examined in vitro chemotaxis and cell spreading under shear stress. Ibrutinib treatment did not inhibit transwell chemotaxis or the ratio of motile adherent cells and arrested cells under

shear stress (**Figure 6J-L**) but markedly reduced the number of spread cells under shear stress of both WT and WASp XLN neutrophils (**Figure 6M).** Together, this data suggests that WASp is one of the targets of Btk for neutrophil spreading mediated by integrin activation as previously shown (31). For cell movement, WASp activation is upstream of PI3K signalling and the L272P and I296T mutations render WASp less dependent on PI3K signalling.

Increased phagocytosis rate but normal killing of bacteria in XLN neutrophils

To examine host defense responses in XLN, we first examined *in vitro* killing of gram negative and gram positive bacteria by WASp XLN neutrophils. We found that killing of *E. coli* or *S. aureus* by WASp XLN neutrophils was intact (**Figure 7A-B**). We next examined the ability of neutrophils to phagocytose fluorescently labelled serum-opsonized *E. coli* and *S. aureus*. WASp L272P and WASp I296T neutrophils had a higher capacity to phagocytose bacteria when compared to WT neutrophils (**Figure 7C-D**). Intracellular ROS production was similar between WT and WASp XLN neutrophils when incubated with heat killed opsonized *E. coli* or *S. aureus* and the cell permeable luminol substrate (**Figure 7E-F**). Intriguingly, when compared to WT neutrophils, WASp L272P and WASp I296T neutrophils had increased intracellular ROS production upon receptor-independent PMA activation (**Figure 7G**). The increased intracellular ROS production in WASp XLN neutrophils was evident also after quenching extracellular superoxide with superoxide dismutase (SOD) (**Supplemental Figure 6A**).

Extracellular ROS produced by translocation of NADPH components to the plasma membrane was measured with lucigenin. When compared to WT neutrophils, WASp L272P and WASp I296T neutrophils had reduced extracellular ROS production upon stimulation with *S. aureus*, fMLP, and PMA (**Figure 7H-J**). To examine if increased cortical F-actin in XLN neutrophils impaired extracellular ROS production, we treated control human and WT murine neutrophils with the actin stabilizing drug jasplakinolide. Upon treatment with jasplakinolide and PMA activation, both human and murine WT neutrophils had lower extracellular ROS production (**Figure 7K**).

Altered granule release in XLN neutrophils

We reasoned that changes in intra- and extracellular ROS may be a result of altered trafficking of granules to the surface. To test this hypothesis, we measured secretion of

neutrophil elastase, that together with other serine proteases such as proteinase 3 and cathepsin G are stored in large quantities in azurophilic granules (32). We used a probe that emits fluorescence upon cleavage by neutrophil elastase. Wildtype and XLN murine neutrophils showed low secretion of elastase in response to fMLP (**Figure 8A**). Upon treatment of neutrophils with cytochalasin B to depolymerize the cortical actin cytoskeleton, XLN neutrophils showed higher elastase secretion when compared to WT neutrophils both in the presence and absence of fMLP (**Figure 8A** and **Supplemental Figure 7A**). Importantly, secretion of CD11b that is present in specific granules, gelatinase granules and secretory vesicles (32) does not require cytochalasin priming. To investigate the effect of WASp L272P and WASp I296T on CD11b distribution in neutrophils, we activated neutrophils with PMA. Upon activation, WT neutrophils upregulated CD11b on their cell surface. When compared to WT bone marrow and blood neutrophils, CD11b surface expression was lower on WASp L272P and WASp I296T neutrophils upon activation (**Figure 8B-C** and **Supplemental Figure 7B-C**). The upregulation of CD11b was also lower in WASp L272P and WASp I296T neutrophils upon stimulation with the neutrophil chemoattractant C5a (**Figure 8D**), whereas shedding/internalization of the C5a receptor (C5aR) was similar in WT and XLN neutrophils (**Supplemental Figure 7D**). The total pool of surface plus intracellular CD11b was similar between WT and WASp XLN neutrophils (**Supplemental Figure 7E-F**), suggesting that decreased surface expression of CD11b in XLN neutrophils was caused by reduced trafficking of CD11b from intracellular vesicles to the cell surface. To examine if increased cortical F-actin in XLN neutrophils impaired translocation of CD11b to the cell surface, we treated control WT murine and human neutrophils with the actin stabilizing drug jasplakinolide. Upon treatment with jasplakinolide and PMA activation, both murine WT and human neutrophils had lower expression of CD11b (**Figure 8E-F**). In contrast to XLN neutrophils, WASp KO neutrophils had decreased cortical F-actin (**Supplemental Figure 7G-H**) and showed increased CD11b cell surface expression upon PMA activation (**Supplemental Figure 5I**). Our mixed bone marrow chimera experiment (**Supplemental Figure 7J**) provided the possibility to examine CD11b expression in WT and XLN neutrophils side by side. When compared to WT neutrophils in the same chimera mouse, WASp L272P and WASp I296T neutrophils in the bone marrow, blood, and spleen had lower surface expression of CD11b (**Supplemental Figure 7J**).

To examine the functional consequence of decreased surface CD11b, we used internal reflection microscopy (IRM) to examine the adhesive surface of neutrophils towards

fibrinogen-coated glass at steady state. When compared to wildtype neutrophils, WASp L272P and WASp I296T neutrophils had smaller adhesive surface area, suggesting reduced integrin mediated firm adhesion (**Figure 8G-H**). The decrease of lamellopodia size (**Supplemental Figure 4F**) was proportional to the decreased adhesion footprint (**Supplemental Figure 7K**).

We next examined CD11b surface expression of neutrophils from the XLN patients. We found that CD11b expression was reduced on XLN neutrophils when compared to C1 and C2 control cells (**Figure 8I**).

Together, this data shows that despite reduced myelopoiesis in XLN, the increased activity of WASp compensated for this dysfunction by WASp localization to the plasma membrane in a constitutively active state that induced increased actin dynamics and elevated neutrophil adhesion and migration.

DISCUSSION

Studies of WASp-deficient neutrophils have revealed the importance of WASp for neutrophil migration and function (29, 31). We reasoned that XLN mutations in WASp may affect multiple steps during neutrophil development in bone marrow and effector functions in tissues. We took a translational approach and combined analysis of neutrophils in XLN patients with two new XLN mouse models that we generated. We found evidence for paucity in myelopoiesis in XLN patients and that the few neutrophils present in peripheral blood showed a hyper-activated phenotype. Interestingly, XLN patients had normal number of neutrophils in saliva, indicating presence of neutrophils at peripheral sites such as the periodontal tissue. Using the XLN mouse models, we found that XLN neutrophils displayed increased chemokine-induced migration and integrin-mediated adhesion under flow and that they accumulated in tissues. We provide molecular evidence in primary neutrophils for that the hyperactivity of XLN neutrophils is caused by constitutive phosphorylation of the critical residue WASp Y293, WASp localization proximal to the plasma membrane, and exposure of the WASp VCA domain that induces actin polymerization even in the absence of receptor stimulation. Our data show that regulated WASp activity by conformational change is required for coordinating cellular signalling to actin dynamics in neutrophils.

We studied human peripheral blood and saliva from two WASp L270P XLN patients (16) and control subjects. As expected (16), blood neutrophil numbers were extremely low in the XLN patients. The XLN patient neutrophils had an activated phenotype as evident by elevated surface expression of gp91 and degranulated morphology. Despite the low blood count in XLN patients, the number of neutrophils in their saliva was normal, suggesting that neutrophils accumulated in tissues. Importantly, this notion is supported by the relatively mild clinical symptoms of XLN patients compared to other types of SCNs. Beel et al. described that patients with the WASp I294T mutation have considerable variation in infectious history, and the severity of their neutropenia did not correlate closely with their susceptibility to infections (15). Ancliff and colleagues reported that a patient with WASp S272P mutation has less severe phenotype than classic SCN and the patient responded well to more modest doses of G-CSF. Moreover, no gingivitis or periodontitis have been detected in XLN patients although this is one of the cardinal clinical symptom in other SCNs (1-3). Our data together with the clinical findings suggests that the granulocyte compartment in XLN patients compensates for the partial myeloid differentiation blockade in the bone marrow. Moreover, the extremely low absolute neutrophil number in blood does not reflect the effector potential of the neutrophil pool.

To understand the pathophysiology of XLN and how activating mutations in WASp affects neutrophils, we generated two independent knock-in mouse models harbouring the corresponding murine XLN mutations WASp L272P and WASp I296T. We followed our XLN mouse colonies for 12 months of age and found no signs of low neutrophil numbers in peripheral blood or any neutrophil-related illness. Neither did we detect any signs of bone marrow failure upon G-CSF administration in XLN mice. Many attempts have been made to generate mouse models for human neutrophil deficiency. Some mouse models show neutropenia, including mice lacking (G6PC)3 or Rac2 (33, 34), but other mouse models have failed to induce neutropenia in mice such as the deficiency of neutrophil elastase (35). It is possible that mouse models fail to capture certain aspects of SCN such as progressive bone marrow failure. Furthermore, penetrance of neutropenia in male carriers of XLN mutation is incomplete which highlights the possibility of epistatic genetic interaction between WASp and other unknown gene variants or environmental effects in XLN pathogenesis which perhaps is not captured by our inbred C57BL/6 mouse model. Notably our mice were kept under specific pathogen free (SPF) conditions, which results in a relatively low homeostatic

blood neutrophil number, also in wildtype mice (36-38). We show that XLN patients had a reduced plasma level of the anti-microbial peptide hCAP18, which is produced during early myelopoiesis, and that WASp L270P $CD34^+$ stem cells and progenitors matured into neutrophils at reduced rate *in vitro*. This result suggests a partial developmental defect in bone marrow (25, 26).

The amino acid sequence of murine and human WASp is 86% identical and the GBD domain is 100% identical. Despite the apparent failure of the two WASp XLN mouse strains to model aberrant myeloid differentiation, we reason that the XLN mouse models are superior to human blood samples to investigate WASp XLN neutrophils *in vitro*. We showed that the extremely low number of granulocytes detected by flow cytometry in human blood or purified by density gradient centrifugation were heavily enriched for eosinophils. This enrichment of eosinophils may bias the interpretation of clinical assays aimed to studying neutrophils in blood samples. We found in primary murine neutrophils that wildtype WASp was present in protein lysates whereas the WASp XLN protein rapidly underwent proteolytic degradation. The degradation of WASp XLN could be prevented by pre-treatment with a potent serine protease inhibitor. This suggests that wildtype WASp was protected from neutrophil proteases during cell lysis, whereas WASp XLN was rapidly degraded when exposed to neutrophil proteases because of its open conformation. Consistent with our data from studies of murine XLN B and T cells with increased load of F-actin (39), WASp XLN mutations caused spontaneous actin polymerisation in neutrophils both in the cytoplasm and in the cortical F-actin network. This shows that the VCA domain of WASp XLN is constantly exposed for binding to the Arp2/3 complex leading to actin polymerization. From studies of N-WASp using *in vitro* systems (19), it has been suggested that WASp in the open conformation may be recruited to membranes by interaction with PIP2. We found that WASp XLN localized proximal to the plasma membrane in primary neutrophils, even in the absence of stimuli. Another predicted consequence of WASp in open conformation is increased phosphorylation of WASp. When the auto-inhibition of WASp is released by Cdc42 and PIP2, the critical Y291 (Y293 in mouse) is exposed and phosphorylated allowing for binding to kinases that prolong the activated, open conformation state of WASp in the absence of Cdc42 (21). We show in primary neutrophils that Y293 was hyper-phosphorylated in WASp L272P and WASp I296T even in the absence of stimuli. High basal L270P phosphorylation has been found previously in COS-7 cells transfected with WASp L270P (40). Interestingly, the phenotype of WASp XLN partially overlaps with that of the phospho-mimicking mutant

WASp Y293E (41). The WASp Y293E mutant induce increased actin polymerisation *in vitro* and the WASp Y293E protein was degraded in protein lysates (41).

Surprisingly, we found that WASp XLN neutrophils migrated to tissues at an increased rate using four different models; *S. aureus* induced peritonitis and dermatitis, thioglycolate induced sterile peritonitis in mixed bone marrow chimeras, and competitive homing experiments. Neutrophil migration into tissue requires active regulation of the actin cytoskeleton. First, neutrophil extravasation requires actin mediated spreading on the activated endothelium which is regulated by integrin outside in signalling. Second, amoeboid migration requires a coordinated regulation of actin polymerisation in pseudopodia and retraction of uropods. Here we show that a high proportion of WASp XLN neutrophils acquired an irregular shaped cortical actin upon activation indicating enhanced actin dynamics. CXCL1 activation of neutrophils caused a rapid transient phosphorylation of WASp Y293, which was more prolonged and had higher amplitude in WASp XLN neutrophils. This increased actin dynamics in WASp XLN neutrophils can be directly connected to increased rate of extravasation in flow chamber assays where we show increased rate of adhesion of WASp XLN neutrophils to beta 2 integrin ligand (ICAM-1) coated surface upon activation with P-selectin and CXCL-1. The increased actin dynamics could be also detected using transwell assays where WASp XLN neutrophils showed increased migration toward C5a, fMLP, and CXCL1 gradients. In transwell assay, WT and WASp XLN neutrophils were equally sensitive to F-actin stabilizing (Jasplakinolide) or disrupting (Cytochalasin B, CK-666) drugs indicating that the dynamics and localization of the actin polymerisation gives advantage to WASp XLN neutrophils. Intriguingly, they were also similarly sensitive to Cdc42 inhibition (ML-141), suggesting that WASp XLN migration is dependent on Cdc42. Finally, WASp XLN neutrophils were less sensitive to the migration inhibiting effect of the PI3K inhibitor wortmannin. Activation-induced relocation of WASp to the plasma membrane was also PI3K dependent and we speculate that WASp relocation and migration are connected. Recent work of Zarbock and colleagues (42) implicates that WASp in neutrophils can be recruited to the plasma membrane via Skap2 which binds PIP3 providing a possible mechanism of wortmannin sensitivity. Finally, by pharmacological inhibiton we found that the hyperphosphorylation of WASp XLN was dependent on Btk, suggesting that WASp is a direct target of Btk.

To address if WASp is involved in regulating host defense properties of neutrophils, we tested bacteria killing, phagocytosis, and ROS production. WT and WASp XLN neutrophils had similar capacity to kill *S. aureus* and *E. coli in vitro*. To further dissect the interaction between neutrophils and bacteria we measured the uptake of opsonized *S. aureus* and *E. coli*. Consistent with increased actin dynamics, WASp XLN neutrophils had enhanced capacity to phagocytose opsonized gram positive and gram negative bacteria. *S. aureus* and *E. coli* mediated intracellular ROS was similar between WT and WASp XLN neutrophils, however, receptor-independent intracellular ROS production was increased in WASp XLN neutrophils indicating enhanced intracellular signalling. In contrast to intracellular ROS, extracellular ROS production was defective in WASp XLN neutrophils when measured after either fMLP, PMA, *S. aureus* stimulation. Since decreased extracellular ROS could be caused by reduced capacity to release intracellular vesicles by WASp XLN neutrophils, we examined surface translocation of CD11b. CD11b surface expression on murine and patient XLN neutrophils was lower than on control neutrophils at steady state and upon stimulation. We could mimic the phenotype of XLN neutrophils by pharmacological stabilization of F-actin using jasplakinolide and we postulate that extracellular ROS and CD11b surface expression negatively correlates with the F-actin content of neutrophils. Severely reduced CD11b expression causes Leukocyte Adhesion Deficiency I (LAD I) (11). Our study suggests that increased actin dynamics with a hyper-migratory response of neutrophils may be associated with moderately lower CD11b expression. The speed of cell migration is a function of attachment strength between the cell and the substratum with maximal migration speed at an intermediate level of cell-substratum adhesiveness (43). Since migration requires cell detachment, we speculate that a small decrease in CD11b expression may lead to increased cell migration.

Our data shows the importance of fine-tuning WASp activity by structural conformation, membrane localization, and tyrosine phosphorylation for normal neutrophil responses. We favour a model suggested by Rosen et al. (21) in which WASp in the open conformation is tyrosine phosphorylated by kinases thus providing a molecular memory of WASp activation leading to actin polymerization. The XLN mutations expose the WASp Y293 residue that can be phosphorylated by kinases such as Btk as we show here. This will lead to sustained WASp activity and the possibility to induce WASp activity further as indicated by our data. We show that WASp Y293 phosphorylation and actin polymerization could be induced in chemokine stimulated XLN neutrophils, suggesting that WASp XLN can have induced activity.

Moreover, we show increased motility of spread cells upon CD11b activation, suggesting increased dynamics of the actin cytoskeleton upon receptor activation and a dynamic contact area on an adhesive surface. The molecular memory model (21) together with our findings from investigation of XLN neutrophils suggests that receptor activation can further enhance the amplitude of WASp activity inside a cell.

Although severe neutrophil defects have been shown in knockout models of WAS, its contribution to disease pathogenesis in WAS is confounded by the profound immune dysregulation in other immune cell compartments. In contrast to WAS patients, the clinical pathogenesis in XLN patients is largely focused on the low neutrophil number in blood. Combining the relatively mild clinical presentation of XLN patients and our study, we propose that XLN neutrophils can compensate for reduced bone marrow output by increased migration into tissues where they are functional. It is possible that increased rate of adhesion by XLN neutrophils in vasculature contributes to relative neutropenia as measured in blood. Our study categorizes XLN as an atypical SCN where low absolute neutrophil count in blood samples does not warrant life-long G-CSF support.

MATERIALS AND METHODS

Patients

We analysed peripheral blood and saliva from two XLN patients, one carrier female, one related female with unknown carrier status, and three healthy volunteers. Peripheral blood was anticoagulated on potassium EDTA or sodium heparin.

Mice

The WASp L272P and WASp I296T knock in strains were generated by Ingenious Targeting Laboratory by insertion of a point mutation into germline *WASp* exon 9; TTG to CCG to generate the Leu-272 to Pro-272 knock-in mutation or ATT to ACT to generate the Iso-296 to Thr-296 knock-in mutation. WASp-L272P mice (C57Bl/6 ES cells, C57Bl/6 background) and WASp-I296T mice (mixed 129Sv and C57Bl/6 ES cells, backcrossed for more than 7 generations to C57Bl/6 background), WKO mice (mixed 129Sv and C57Bl/6 ES cells, backcrossed at least 9 generations to C57Bl/6 background) (44), and littermate WT controls were bred and maintained at the animal facility of the Department of Microbiology, Tumor

and Cell Biology at Karolinska Institutet under specific pathogen-free conditions. The Lifeact-EGFP transgenic mouse (28) was originally obtained from Roland Wedlich-Söldner and was crossed into WASp-L272P mice and WASp-I296T mice. Male mice were used 6-12 weeks of age.

Neutrophil differentiation of human CD34+ progenitors

CD34+ cells were purified from peripheral blood mononuclear cells with magnetic bead positive selection (Miltenyi Biotec) and cultured with IL-3, SCF, and G-CSF for 13 days (45).

Neutrophils

Murine bone marrow neutrophils were isolated as described in Mocsai et al. (46). Briefly, bone marrow from femur and tibia was flushed and red blood cells were lysed with hypotonic salt solution. Bone marrow cell suspension was purified with 62.5 % density discontinuous Percoll (GE Healthcare Life Sciences) gradient centrifugation. The neutrophil containing fraction contains over 85% neutrophil granulocytes. When higher purity was needed, neutrophils were isolated with magnetic bead negative selection (Miltenyi Biotec). Human neutrophils were purified according to Nauseef et al. (27) with dextran sedimentation and Ficoll-Hypaque density gradient centrifugation. .

Bone marrow chimera

For generation of mixed bone marrow chimeras, 1×10^7 total bone marrow cells containing WASp L272P or WASp I296T bone marrow cells (expressing CD45.2) and WT bone marrow cells (expressing CD45.1) at a 3:1 ratio were transplanted via intravenous injection into lethally irradiated (13 Gy) WT C57BL/6 recipient animals.

***In vivo* homing experiments**

The air pouch was created in F1(CD45.1xCD45.2) mice by repeatedly injecting sterile air subcutaneously. At day 6 after initial injection, 1×10^7 WT (CD45.1) and WASp L272P, WASp I296T, or WKO neutrophils were injected at a 1:1 ratio intravenously into the F1(CD45.1xCD45.2) recipients. Five hours after fMLP and TNFα injection into the air pouch, mice were sacrificed and blood, bone marrow, spleen, and lavage from the air pouch was analyzed by flow cytometry. Grafted neutrophils (CD45.1 or CD45.2 single positive) were counted and the following normalized and log transformed values have been plotted: $Log_2[Mut/WT]_{norm}=Log_2[(Mut/WT)/(Mut/WT)_{grafted}]$-Avg(Log2[($WT_{CD45.2}/WT_{CD45.1}$)/

($WT_{CD45.2}/WT_{CD45.1})_{grafted}$]). The first logarithmic part in the equation represents the normalized migration ratio of mutant neutrophils compared to WT neutrophils (normalized to the original grafted ratio, quantified each time before the experiment) and the second average Log2 value represents the migration bias caused by the CD45.1/.2 isoforms as determined in WT neutrophils.

ROS

Neutrophils $5x10^5$ in HBSS/5% FCS were incubated in 96-well white flat bottom plates (Thermo Fisher Scientific) for 30 minutes at 37°C with Luminol (Sigma; at 56 μM final concentration) or Lucigenin (Sigma; at 50 μM final concentration). ROS induced chemiluminescent signals were measured with luminometer (BMG Labtech) upon activation of the neutrophils with fMLP (final 3 μM), PMA (final 100ng/ml), or heat-killed serum opsonized *S. aureus* (1 neutrophil:10 bacteria).

Phagocytosis

Bone marrow derived neutrophils and serum opsonized A488 labelled *E. coli* or *S. aureus* (Thermo Fischer Scientific) were co-incubated at a ratio of 1:5 at 37˚C. Samples were taken at various time points and the phagocytosis rate of bacteria was measured by flow cytometry.

In vitro killing of bacteria

Mouse serum opsonized *E.coli* (WA321; DSMZ collection) or *S.aureus* (Seattle 1945; DSMZ collection) was incubated in a rotating tube at 37C with neutrophils for the indicated time and ratio of neutrophils vs. bacteria. Neutrophils were lysed in hypotonic solution, the solution was DNase I (Roche) digested and spread at various dilutions on Luria-Bertani or blood agar plates. Colony forming units (CFUs) were enumerated after 12 h incubation of plates at 37C. Data depicted as percentage of CFU decrease in neutrophil-bacteria mixtures compared to bacteria without neutrophils.

Transwell migration assay

Bone marrow neutrophils in HBSS/5% FCS were added to the upper chambers of transwells (3.0 μm pore size) (Costar, Cambridge, MA). The lower chambers were filled with HBSS, 5% FBS and different concentrations of C5a, CXCL1, fMLP. Plates were incubated 2h at 37˚C and number of transmigrated cells was measured by flow cytometry.

Flow cytometry

Single cell suspensions were immuno-labelled with the following antibodies after blocking non-specific binding with CD16/32 (93) (mouse) or Human BD Fc Block (BD Pharmingen) and 20% rabbit serum: CD15 (W6D3), CD16 (3G8), gp91phox (7D5), CD11b (M1/70), Siglec-8 (7C9), CD45 (HI30), Ly6G (1A8), C5aR (20/70), CD45.1 (A20), CD45.2 (104). DAPI staining was used to exclude dead cells. Cells were acquired with LSR Fortessa (Becton Dickinson) or ImageStream^X Mark II Imaging Flow Cytometer (Amnis). Analyses were made using FlowJo software (TreeStar Inc.) and IDEAS v.6 software (Amnis).

Western blot

Neutrophils were lysed in Triton-X-100 lysis buffer after a 10 min pre-incubation of cells with the serine protease inhibitor 5mM diisopropylfluorophosphate (DPF; Sigma-Aldrich,St. Louis, USA). Murine neutrophil protein lysates or immunoprecipitated lysates were run with 4-12% SDS-PAGE gel electrophoresis in MES buffer under reducing condition using the Bolt gel system (Thermo Fisher Scientific). Blots were developed with anti-WASp (Santa Cruz; B-9 and F-8 antibodies) and anti-WASP phospho-Y293 (Abcam).
Human hCAP18 was detected in plasma as described before (26) .

Light Microscopy

For phalloidin and CD11b staining, bone marrow derived neutrophils in cell suspension or adherent on fibrinogen were fixed (PFA Fixation buffer, BioLegend), washed and permeabilized (Biolegend, San Diego, USA). Cells were stained with an Alexa-488 or Alexa-647-labelled phalloidin (ThermoFisher Scientific, Waltham,USA), and CD11b (clone M1/70, BioLegend). Labelled cells were stained with secondary anti-rat Alexa-555 antibody (ThermoFisher Scientific, Waltham,USA), mounted on glass coverslips in Vectashield mounting medium with DAPI (Vector Laboratories, Burlingame, USA). Slides were imaged using a Leica TCS SP5 confocal microscope, or Leica DMRE (Leica). Analysis of cortical actin was performed using the Fiji software (47).

Electron microscopy

For Transmission electron microscopy (TEM), cells were fixed in 2.5 % glutaraldehyde in 0.1M phosphate buffer, pH 7.4 then postfixed in 2% osmium tetroxide (TAAB, Berks, England). After embedding in LX-112 (Ladd, Burlington, Vermont, USA), ultrathin sections (approximately 50-60 nm) were cut and contrasted with uranyl acetate followed by lead

citrate and examined in a Hitachi HT 7700 election microscope (Tokyo, Japan) at 80 kV. Digital images were taken by using a Veleta camera (Olympus Soft Imaging Solutions, GmbH, Münster, Germany).

For Scanning electron microscopy (SEM), specimens were fixed by immersion in 2,5 % glutaraldehyde in 0.1M PB (pH 7.4), dried and coated with 10 nm Platinum (Q150T ES, West Sussex, UK). The specimens were analyzed in an Ultra 55 field emission scanning electron microscope (Zeiss, Oberkochen, Germany) at 3 kV.

Saliva

Saliva was extensively washed, stained with fluorescent antibodies, fixed with paraformaldehyde and successively filtered through 70, 40, 20, and 10µm filters.

Cytospin and Staining

Cytospin (Shandon Scientific Co., Ltd., London) slides were stained with Differential Quik Stain (Polysciences Inc., Warrington, USA) according to the manufacturer's protocol.

Flow chamber

µ-Slide $I^{0.4}$ (IBIDI GmbH, Munich, Germany) plastic flow chambers were coated with rmP-selectin (Biolegend, San Diego, USA), rmICAM-1 (R&D Sytems, Minneapolis, USA), and rmCXCL-1(Biolegend, San Diego, USA). Coated plastic flow chambers were perfused with bone marrow neutrophils at 0,1 dyn/cm^2, than shear stress was stepwise increased to indicated values every 30 seconds using a syringe pump (Chemyx Inc., Stafford, USA). Images were taken with a Zeiss Axio Observer.Z1 microscope (Zeiss, Oberkochen, Germany).

Statistics

Analysis for statistical significance ($p<0.05$) with two-tailed Student's t test, one-way ANOVA with posthoc Bonferroni correction, or two-way ANOVA as indicated at the specific experiments were performed with GraphPad Prism (GraphPad Software, Inc., La Jolla, USA). Error bars represent SEM or in ROS experiments, SD.

Study Approval

The study was approved by the Institutional Review Board of UZ Leuven and a written consent form was obtained from all individuals. All animal experiments were performed after

approval from the local ethical committee (the north Stockholm district court, permit N77/13 and N272/14).

ACKNOWLEDGEMENTS

The authors are grateful to the XLN patients and their family for supporting our study. We would like to thank for the valuable comments and/or technical instructions from Nancy Boeck and Sanne Smits at UZ Leuven, Anne van der Does and Lennart Lindbom at Karolinska Institutet, and Siobhan Burns and Adrian Thrasher at University College London. We are grateful to the staff of the Department of Microbiology Tumor and Cell biology animal facility for their technical support and Kjell Hultenby for the electron microscopy.
This work was supported by a postdoctoral fellowship from the Cancer Society to M.K., a postdoctoral fellowship from the Childhood Cancer Society to J.R, a clinical postdoctoral fellowship from the Swedish Society of Medical Research to H.B., a postdoctoral fellowship from Olle Engqvist Byggmästare to M.H., a PhD fellowship from Fundação para a Ciência e a Tecnologia #SFRH/BD/47926/2008 to M.A.P.B., as well as O. E. and Edla Johanssons foundation, Lars Hierta Memorial Foundation, Tore Nilsson Foundation to M.K., Grochinsky foundation to H.B., the Swedish Medical Society to H.B. and L.S.W., Swedish Research Council, Cancer Society, Childhood Cancer Society, the European Commission 7th framework program Marie Curie reintegration grant (#249177), Åke Olsson foundation, Jeansson foundation, Groschinsky Foundation, Åke Wiberg Foundation, Bergvall Foundation, King Gustaf V's 80-year Foundation, and Karolinska Institutet to L.S.W. L.S.W. is a Ragnar Söderberg fellow in Medicine.

AUTHOR CONTRIBUTION

M.K. and L.S.W. designed the research, M.K., J.R., J.S.K., H.W., C.G., M.T., P.D., H.B., L.K., J.J., M.H., M.A.P.B., C.I.M.D., A.B, and K.P. performed the experiments and analysed the data, S.L., D.P.L., and S.B.S contributed with critical tools, W.S. supervised the imaging analysis; P.V. provided XLN patient samples and analysed patient data, M.K. and L.S.W. wrote the manuscript, and all authors edited the manuscript.

Conflict-of-interest disclosure: The authors have declared that no conflict of interest exists.

REFERENCES

1. Skokowa J, Dale DC, Touw IP, Zeidler C, and Welte K. Severe congenital neutropenias. *Nat Rev Dis Primers.* 2017;3:17032.
2. Dale DC, and Link DC. The many causes of severe congenital neutropenia. *N Engl J Med.* 2009;360(1):3-5.
3. Klein C. Genetic defects in severe congenital neutropenia: emerging insights into life and death of human neutrophil granulocytes. *Annu Rev Immunol.* 2011;29:399-413.
4. Dinauer MC. Primary immune deficiencies with defects in neutrophil function. *Hematology Am Soc Hematol Educ Program.* 2016;2016(1):43-50.
5. van de Vijver E, van den Berg TK, and Kuijpers TW. Leukocyte adhesion deficiencies. *Hematol Oncol Clin North Am.* 2013;27(1):101-16, viii.
6. Nemeth T, and Mocsai A. Feedback Amplification of Neutrophil Function. *Trends Immunol.* 2016;37(6):412-24.
7. Kolaczkowska E, and Kubes P. Neutrophil recruitment and function in health and inflammation. *Nat Rev Immunol.* 2013;13(3):159-75.
8. Lomakina EB, Marsh G, and Waugh RE. Cell surface topography is a regulator of molecular interactions during chemokine-induced neutrophil spreading. *Biophys J.* 2014;107(6):1302-12.
9. Nunoi H, Yamazaki T, Tsuchiya H, Kato S, Malech HL, Matsuda I, et al. A heterozygous mutation of beta-actin associated with neutrophil dysfunction and recurrent infection. *Proc Natl Acad Sci U S A.* 1999;96(15):8693-8.
10. Record J, Malinova D, Zenner HL, Plagnol V, Nowak K, Syed F, et al. Immunodeficiency and severe susceptibility to bacterial infection associated with a loss-of-function homozygous mutation of MKL1. *Blood.* 2015;126(13):1527-35.
11. Keszei M, and Westerberg LS. Congenital defects in neutrophil dynamics. *J Immunol Res.* 2014;2014:303782.
12. Moulding DA, Record J, Malinova D, and Thrasher AJ. Actin cytoskeletal defects in immunodeficiency. *Immunol Rev.* 2013;256(1):282-99.
13. Procaccio V, Salazar G, Ono S, Styers ML, Gearing M, Davila A, et al. A mutation of beta -actin that alters depolymerization dynamics is associated with autosomal dominant developmental malformations, deafness, and dystonia. *Am J Hum Genet.* 2006;78(6):947-60.
14. Riviere JB, van Bon BW, Hoischen A, Kholmanskikh SS, O'Roak BJ, Gilissen C, et al. De novo mutations in the actin genes ACTB and ACTG1 cause Baraitser-Winter syndrome. *Nat Genet.* 2012;44(4):440-4, S1-2.
15. Beel K, Cotter MM, Blatny J, Bond J, Lucas G, Green F, et al. A large kindred with X-linked neutropenia with an I294T mutation of the Wiskott-Aldrich syndrome gene. *Br J Haematol.* 2009;144(1):120-6.
16. Devriendt K, Kim AS, Mathijs G, Frints SG, Schwartz M, Van Den Oord JJ, et al. Constitutively activating mutation in WASP causes X-linked severe congenital neutropenia. *Nat Genet.* 2001;27(3):313-7.
17. Ancliff PJ, Blundell MP, Cory GO, Calle Y, Worth A, Kempski H, et al. Two novel activating mutations in the Wiskott-Aldrich syndrome protein result in congenital neutropenia. *Blood.* 2006;108(7):2182-9.
18. Kim AS, Kakalis LT, Abdul-Manan N, Liu GA, and Rosen MK. Autoinhibition and activation mechanisms of the Wiskott-Aldrich syndrome protein. *Nature.* 2000;404(6774):151-8.
19. Rohatgi R, Ho HY, and Kirschner MW. Mechanism of N-WASP activation by CDC42 and phosphatidylinositol 4, 5-bisphosphate. *J Cell Biol.* 2000;150(6):1299-310.

20. Rohatgi R, Ma L, Miki H, Lopez M, Kirchhausen T, Takenawa T, et al. The interaction between N-WASP and the Arp2/3 complex links Cdc42-dependent signals to actin assembly. *Cell.* 1999;97(2):221-31.
21. Torres E, and Rosen MK. Contingent phosphorylation/dephosphorylation provides a mechanism of molecular memory in WASP. *Mol Cell.* 2003;11(5):1215-27.
22. Cory GO, Garg R, Cramer R, and Ridley AJ. Phosphorylation of tyrosine 291 enhances the ability of WASp to stimulate actin polymerization and filopodium formation. Wiskott-Aldrich Syndrome protein. *J Biol Chem.* 2002;277(47):45115-21.
23. Guinamard R, Aspenstrom P, Fougereau M, Chavrier P, and Guillemot JC. Tyrosine phosphorylation of the Wiskott-Aldrich syndrome protein by Lyn and Btk is regulated by CDC42. *FEBS Lett.* 1998;434(3):431-6.
24. Fujimoto H, Sakata T, Hamaguchi Y, Shiga S, Tohyama K, Ichiyama S, et al. Flow cytometric method for enumeration and classification of reactive immature granulocyte populations. *Cytometry.* 2000;42(6):371-8.
25. Sorensen O, Arnljots K, Cowland JB, Bainton DF, and Borregaard N. The human antibacterial cathelicidin, hCAP-18, is synthesized in myelocytes and metamyelocytes and localized to specific granules in neutrophils. *Blood.* 1997;90(7):2796-803.
26. Ye Y, Carlsson G, Karlsson-Sjoberg JM, Borregaard N, Modeer TU, Andersson ML, et al. The antimicrobial propeptide hCAP-18 plasma levels in neutropenia of various aetiologies: a prospective study. *Sci Rep.* 2015;5:11685.
27. Quinn MT, DeLeo FR, and Bokoch GM. Neutrophil methods and protocols. Preface. *Methods Mol Biol.* 2007;412:vii-viii.
28. Riedl J, Flynn KC, Raducanu A, Gartner F, Beck G, Bosl M, et al. Lifeact mice for studying F-actin dynamics. *Nat Methods.* 2010;7(3):168-9.
29. Zhang H, Schaff UY, Green CE, Chen H, Sarantos MR, Hu Y, et al. Impaired integrin-dependent function in Wiskott-Aldrich syndrome protein-deficient murine and human neutrophils. *Immunity.* 2006;25(2):285-95.
30. Sakuma C, Sato M, Takenouchi T, Chiba J, and Kitani H. Critical roles of the WASP N-terminal domain and Btk in LPS-induced inflammatory response in macrophages. *PLoS One.* 2012;7(1):e30351.
31. Volmering S, Block H, Boras M, Lowell CA, and Zarbock A. The Neutrophil Btk Signalosome Regulates Integrin Activation during Sterile Inflammation. *Immunity.* 2016;44(1):73-87.
32. Borregaard N, and Cowland JB. Granules of the Human Neutrophilic Polymorphonuclear Leukocyte. *Blood.* 1997;89(10):3503-21.
33. Schaffer AA, and Klein C. Animal models of human granulocyte diseases. *Hematol Oncol Clin North Am.* 2013;27(1):129-48, ix.
34. Schaffer AA, and Klein C. Genetic heterogeneity in severe congenital neutropenia: how many aberrant pathways can kill a neutrophil? *Curr Opin Allergy Clin Immunol.* 2007;7(6):481-94.
35. Belaaouaj A, McCarthy R, Baumann M, Gao Z, Ley TJ, Abraham SN, et al. Mice lacking neutrophil elastase reveal impaired host defense against gram negative bacterial sepsis. *Nat Med.* 1998;4(5):615-8.
36. von Vietinghoff S, and Ley K. Homeostatic regulation of blood neutrophil counts. *J Immunol.* 2008;181(8):5183-8.
37. TheJacksonLaboratory. Hematological survey of 11 inbred strains of mice. MPD:Jaxpheno4.
38. Wakeman L, Al-Ismail S, Benton A, Beddall A, Gibbs A, Hartnell S, et al. Robust, routine haematology reference ranges for healthy adults. *Int J Lab Hematol.* 2007;29(4):279-83.

39. Westerberg LS, Meelu P, Baptista M, Eston MA, Adamovich DA, Cotta-de-Almeida V, et al. Activating WASP mutations associated with X-linked neutropenia result in enhanced actin polymerization, altered cytoskeletal responses, and genomic instability in lymphocytes. *J Exp Med.* 2010;207(6):1145-52.
40. Park H, and Cox D. Cdc42 regulates Fc gamma receptor-mediated phagocytosis through the activation and phosphorylation of Wiskott-Aldrich syndrome protein (WASP) and neural-WASP. *Mol Biol Cell.* 2009;20(21):4500-8.
41. Blundell MP, Bouma G, Metelo J, Worth A, Calle Y, Cowell LA, et al. Phosphorylation of WASp is a key regulator of activity and stability in vivo. *Proceedings of the National Academy of Sciences.* 2009;106(37):15738-43.
42. Boras M, Volmering S, Bokemeyer A, Rossaint J, Block H, Bardel B, et al. Skap2 is required for β₂ integrin–mediated neutrophil recruitment and functions. *J Exp Med.* 2017;214(3):851-74.
43. DiMilla PA, Stone JA, Quinn JA, Albelda SM, and Lauffenburger DA. Maximal migration of human smooth muscle cells on fibronectin and type IV collagen occurs at an intermediate attachment strength. *J Cell Biol.* 1993;122(3):729-37.
44. Snapper SB, Rosen FS, Mizoguchi E, Cohen P, Khan W, Liu CH, et al. Wiskott-Aldrich syndrome protein-deficient mice reveal a role for WASP in T but not B cell activation. *Immunity.* 1998;9(1):81-91.
45. Gupta D, Shah HP, Malu K, Berliner N, and Gaines P. Differentiation and characterization of myeloid cells. *Curr Protoc Immunol.* 2014;104:Unit 22F 5.
46. Mocsai A, Zhang H, Jakus Z, Kitaura J, Kawakami T, and Lowell CA. G-protein-coupled receptor signaling in Syk-deficient neutrophils and mast cells. *Blood.* 2003;101(10):4155-63.
47. Schindelin J, Arganda-Carreras I, Frise E, Kaynig V, Longair M, Pietzsch T, et al. Fiji: an open-source platform for biological-image analysis. *Nat Methods.* 2012;9(7):676-82.

FIGURE LEGENDS

Figure 1. Severe neutropenia with hyper-activated neutrophils in the blood of XLN patients. (A) Forward and side scatter flow cytometer plots of RBC lysed blood from WASp L270P XLN patients (X1 and X2), their mutation carrier mother (M), their sister with unknown carrier status, and two healthy male controls (C1 and C2). Granulocyte (Gr), monocyte (Mo), and lymphocyte (Ly) gates are marked with circles. (B) CD15 vs. CD16 staining of whole blood granulocytes. Eo: eosinophils; Neu: neutrophils. (C, D) Granulocyte and neutrophil numbers in blood counted (from Fig.1A-B populations) with flow cytometry using counting beads. (E) hCAP18 expression in serum as determined by Western blot. Serum from SCN1 (ELANE) and SCN3 (HAX1) patients severed as references. (F) Densitometry of hCAP18 blots indicated as percentage density of 1μg/ml hCAP18 reference sample. BD: below detection limit. (G) Percentage and number of CD34+ hematopoietic progenitors in the blood of C2, X1, X2, M, and C3 (female control). (H) Composition of in vitro differentiated myeloid liquid cultures from CD34+ blood cells.

Figure 2. XLN neutrophils are hyper-activated in blood and they are at normal number in saliva. (A) Representative transmission electron microscopy images of neutrophils from gradient purified granulocyte preparation. g: electron-dense granules. (B-C) Gp91phox expression on mature neutrophils (Granulocytes-Eosinophils/CD16HICD11bHI) from WASp L270P XLN patients (X1,X2) and two healthy male controls (C1,C2) before (B) or after (C) PMA stimulation and analyzed by flow cytometry. (D - left panel) Representative imaging flow cytometer plots of CD45 vs. CD15 staining and morphology parameters of Draq5 stained nuclei (circularity vs. aspect ratio). (D - middle panel). Example images of neutrophils ($CD45^{+}CD15^{hi}$ $Draq5[Aspect\ ratio]^{lo}$ $Draq5[Circularity]^{lo}$) taken with imaging flow cyctometer. (D - right panel) Quantitative analysis of neutrophil number/ml saliva.

Figure 3. Increased polymerized actin, WASp Y293 phosphorylation, decreased WASp stability, and altered surface topography in mouse models of XLN. (A) Genomic organization, locations and sequences of the introduced I296T and L272P mutations in the mouse *WASp* gene. (B, C) Protein expression of WASp in lysates of WT, WASp L272P, WASp I296T, and WASp KO (WKO) peritoneal neutrophils with or without pretreatment of cells with diisopropylfluorophosphate (DPF). WASp was detected by western blotting (WB). #: unknown protein. n=3 experiments.(D) Protein expression (upper panel) and Y293 phosphorylation (lower panel) of WASp in WKO, WT, WASp L272P, and WASp I296T in immunoprecipitated protein lysates of bone marrow neutrophils. n=3 experiments.(E) FACS plot of $Ly6G^{+}CD11b^{+}$ neutrophils in mouse peripheral blood. F-actin content of neutrophils was measured with fluorescently labeled phalloidin and flow cytometry. A representative image of three individual blood samples per genotype. (F) Quantitative analysis of cortical and cytoplasmic F-actin, labelled with phalloidin (red), in bone marrow neutrophils. Outlines of cells were recognized by Fiji software and the cortex defined by a ring encompassing the outline. Integrated fluorescent intensity in the ring area and within the ring was measured and values from individual cells were plotted. CFSE labeling (for all genotypes both labelled and unlabeled samples) was used to differentiate between genotypes in each individual field. Data was normalized for the average of WT cytoplasmic signal (100%). Scale bar = 20μM. WASp

I296T (n = 752) vs. WT (n = 482); WASp L272P (n = 256) vs. WT (n = 231). Mean±SD. Unpaired, 2-tailed Student's t-test. (G) Surface structure of WT, WASp L272P, and WASp I296T neutrophils. Cells were isolated from bone marrow, fixed in paraformaldehyde and photographed with scanning electron microscopy (SEM). The percentage of cells with dense surface ruffles (d) were counted manually. Scale bar = 2μM. ****: $p<0.0001$.

Figure 4. Increased rate of migration of WASp L272P and WASp I296T neutrophils to the spleen and to the inflammation site *in vivo*. (A) Neutrophil numbers in ears of WT and WASp L272P mice 6h after induction of dermatitis with *S. aureus* (10^6 CFU) injection. Mean±SEM. Unpaired, 2-tailed Student's t-test; WT n=8; WASp L272P n=8/group. (B) WT and WASp I296T neutrophil numbers in peritoneum 24h after injection of *S. aureus* ($20x10^6$ CFU). Mean±SEM. Unpaired, 2-tailed Student's t-test; WT n=7; WASp I296T n=7/group. (C) WASp L272P/CD45.1 WT (left panel) and WASp I296T/CD45.1 WT (right panel) neutrophil ratios in various organs in mixed bone marrow chimera mice were normalized with their original bone marrow reconstitution ratio (CD45.2/CD45.1) and plotted with logarithmic scale. Mean±SEM, One-way ANOVA with Bonferroni correction; WASp L272P/CD45.1: WT n(bone)=9; n(blood)=22; n(spleen)=11; n(peritoneum)=7; WASp I296T/CD45.1: WT n(bone)=14; n(blood)=21; n(spleen)=14; n(peritoneum)=7/group. (D) *In vivo* homing of WASp L272P (CD45.2), WASp I296T (CD45.2) and CD45.1 WT cells into various tissues was measured 5h after i.v. injection of bone marrow neutrophil grafts. Graft neutrophils (CD45.1+ or CD45.2+ single positive) were counted in blood, bone marrow, spleen, and airpouch lavage. The normalization formula is explained in materials and methods. Pool of at least 2 experiments per genotype. Mean±SEM, One-way ANOVA with Bonferroni correction; WT n=12; WASp I296T n=20; WASp L272P n=21; WKO n=6/group.

Figure 5. Increased actin dynamics and spreading on ICAM-1 in WASp XLN neutrophils. (A) Live cell actin kinetics after neutrophil activation with fMLP was quantified by imaging flow cytometer. Plot of circularity and aspect ratio (upper panel) was calculated on EGFP images. Example images (middle panel) show WT x Lifeact-EGFP cells with increasing circularity. Ratio of irregular (GFP $[\text{Aspect ratio}]^{lo}$ GFP$[\text{Circularity}]^{lo}$) shaped cells as the function of time (lower panel) . Kinetics was calculated after binning data to 30 sec timeframes. >15000 cells / each genotype; 2 independent experiments per genotype. (B) Kinetics of WASp Y293 phosphorylation upon CXCL1 treatment was quantified with imaging flow cytometer after intracellular staining of phospho-Y293 WASp. Phospho-Y293 WASp signal was depicted as fold change of pY293 integrated intensity over background (secondary antibody staining only). n=3, n=4 experiments. (C) Kinetics of F-actin polymerisation upon CXCL1 treatment was quantified with phalloidin staining and flow cytometer. n=3, n=3 experiments. (D) rmP-selectin, rmICAM-1, and rmCXCL-1 coated plastic flow chambers were perfused with bone marrow neutrophils at 0,1 dyn/cm^2. Representative images were taken after increasing flow rate to 2 dyn/cm^2. Motility was assessed by overlaying 10 consecutive frames. (E) Number of arrested cells were counted and depicted as % of arrested cells at 0,1 dyn/cm^2 after increasing flow rate stepwise with 30 sec of run at each indicated sheer stress. n=3, n=3 experiments. (F) Ratio of spread cells at increasing flow rate. (G) Neutrophils in rmP-selectin, rmICAM-1, and rmCXCL-1 coated

plastic flow chambers at 2 dyn/cm^2 shear stress. Black tracks indicate the motility of adherent cells within a 20 minute time period. n=3 images/genotype.

Data is represented as mean±SEM. One-way or two-way ANOVA was used and Bonferroni multiple comparison test for statistical significance. *: p<0.05, **: p<0.01, ***: p<0.001, ****: p<0.0001.

Figure 6. Increased *in vitro* migration, membrane translocation and Btk dependent phosphorylation of WASp in XLN neutrophils. (A, B, C) Migration of WT vs. WASp L272P (left panel) and WASp I296T (right panel) bone marrow neutrophils towards different concentrations of C5a, CXCL1, fMLP in transwell plates. Transmigrated cell numbers were measured by flow cytometry. n=3, n=3 experiments/chemoattractant. (D, E) WT (CD45.1) and WASp XLN (CD45.2) neutrophils were mixed 1:1 ratio in the upper well of a transwell plate and incubated for 10 min with various inhibitors. Migration rate towards C5a or CXCL1 was quantitated with flow cytometry. n=2 experiments. (F) WASp intracellular expression was measured by imaging flow cytometer. WASp intracellular distribution was assessed by calculating ratios of plasma membrane proximal (determined by Ly6G surface staining) WASp and WASp in the total cell in flow cytometer images. Mean+SEM of at least 198 neutrophils. n=3 experiments. (G) WASp and phospho-Y293 WASp proteins in SRC1 and Wortmannin pretreated neutrophils were measured by Western blot. n=2. (H) WASp and phospho-Y293 WASp in WASp L272P neutrophils before and after Ibrutinib treatment. n=3. (I) WASp Y293 phosphorylation upon CXCL1 activation with or without Ibrutinib treatment measured with flow cytometry. n=3. (J) Transwell migration of WT and WASp I296T neutrophils towards C5a (0.125µg/ml), fMLP (3µM), and CXCL1 (0.25 µg/ml) after incubation with the indicated concentrations of Ibrutinib. n=3. (K) Ratio of motile cells among adherent cells on rmP-selectin, rmICAM-1, and rmCXCL-1 under flow as on Figure 5G. (L) Number of arrested cells were counted and depicted as % of arrested cells at 0,1 dyn/cm^2 as on Figure 5E. (M) Ratio of spread cells at increasing flow rate as on Figure 5F. n=3, n=2 experiments. Data is represented as mean±SEM. One-way or two-way ANOVA was used for statistical significance. *: p<0.05, **: p<0.01, ***: p<0.001, ****: p<0.0001.

Figure 7. Increased phagocytosis rate, normal killing of bacteria and dysregulated ROS responses in XLN neutrophils. *E.coli* (A) or *S.aureus* (B) killing capacity of WT and WASp XLN neutrophils was assessed by co-incubating serum opsonized bacteria and neutrophils at a ratio of 1:5 (*E.coli* : neutrophil) for 60 minutes (A) or 1:1 (*S.aureus* : neutrophil) for 60 and 90 minutes in upper and lower panel respectively (B). n=3, n=3 experiments with each bacteria. (C, D) Phagocytosis of Alexa488 labelled serum opsonized *E. coli* (C) and *S. aureus* (D) by WT WASp XLN neutrophils measured by flow cytometry. n=3, n=3 experiments with each bacteria. (E, F, G) Intracellular ROS (IC ROS) measured with luminol chemiluminescence in murine bone marrow neutrophils upon stimulation with E.coli (n=8) (E), *S.aureus* (n=10) (F), or PMA (n=18). n=4, Mean±SD, Two-way ANOVA. (H, I, J) Extracellular ROS (EC ROS) was measured using a lucigenin chemiluminescence assay in murine bone marrow neutrophils upon stimulation with (H) heat-killed serum opsonized *S. aureus* (n=18), (I) fMLP (n=4), or (J) PMA (n=26). n=4, Mean±SD, Two-way ANOVA. (K) Extracellular ROS was measured upon PMA stimulation of murine (upper panel) and human

healthy donor (lower panel) neutrophils with or without pre-treatment with jasplakinolide. n=5, Mean±SD .*: p<0.05, **: p<0.01, ***: p<0.001, ****: p<0.0001.

Figure 8. Altered granule release in XLN neutrophils. (A) Neutrophil elastase secretion by WT and WASp I296T neutrophils was measured with fluorescent detection of the cleavage of MeOSuc-AAPV-AMC substrate after 90 min activation with 10 µM fMLP in the presence of 5µg/ml Cytochalasin B (CyB). n=4, n=3 experiments. (B, C) Upregulation of CD11b upon activation of bone marrow derived neutrophils with PMA (left panel) . Data is represented as percentage of WT unstimulated signal. Percentage of cells above arbitrary baseline MFI of CD11b (right panel) . Bonferroni corrected t-test. n=4, n=4 experiments. (D) CD11b expression of bone marrow derived neutrophils upon C5a stimulation. Two-way ANOVA. n=3. (E, F) CD11b expression on PMA activated murine (E) and human (F) neutrophils. When indicated, neutrophils were pre-incubated 30 min with jasplakinolide. Murine: n=3; human: n=2. (G) Interference reflection microscopy (IRM) images of 5 minutes fMLP activated, adherent neutrophils on fibrinogen coated glass. Scale bar: 10µm. (H) Quantification of adhesion contact area on IRM images. Minimum count of 14 fields per genotype, Mann-Whitney test. n=4 experiments. (I) CD11b expression on mature neutrophils (Granulocytes-Eosinophils/CD16HICD11bHI) from WASp L270P XLN patients (X1,X2) and two healthy male controls (C1,C2) analyzed by flow cytometry. Unless otherwise indicated , data is represented as mean±SEM. One-way or two-way ANOVA was used to test statistical significance. *: p<0.05, **: p<0.01, ***: p<0.001, ****: p<0.0001.

Figure 1

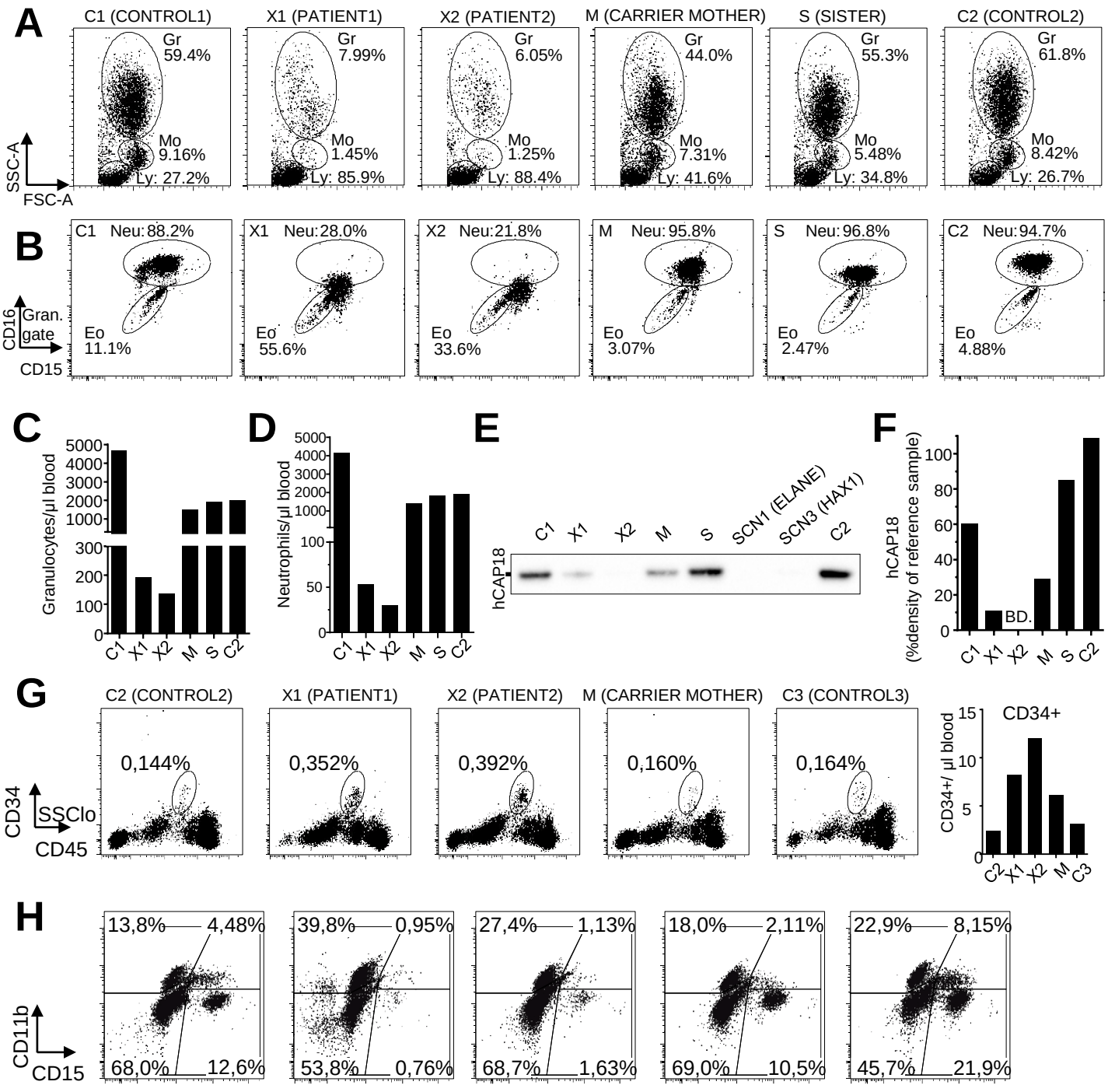

Figure 1. Severe neutropenia with hyper-activated neutrophils in the blood of XLN patients. (A) Forward and side scatter flow cytometer plots of RBC lysed blood from WASp L270P XLN patients (X1 and X2), their mutation carrier mother (M), their sister with unknown carrier status, and two healthy male controls (C1 and C2). Granulocyte (Gr), monocyte (Mo), and lymphocyte (Ly) gates are marked with circles. (B) CD15 vs. CD16 staining of whole blood granulocytes. Eo: eosinophils; Neu: neutrophils. (C, D) Granulocyte and neutrophil numbers in blood counted (from Fig.1A-B populations) with flow cytometry using counting beads. (E) hCAP18 expression in serum as determined by Western blot. Serum from SCN1 (ELANE) and SCN3 (HAX1) patients severed as references. (F) Densitometry of hCAP18 blots indicated as percentage density of 1µg/ml hCAP18 reference sample. BD: below detection limit. (G) Percentage and number of CD34+ hematopoietic progenitors in the blood of C2, X1, X2, M, and C3 (female control). (H) Composition of in vitro differentiated myeloid liquid cultures from CD34+ blood cells.

Figure 2

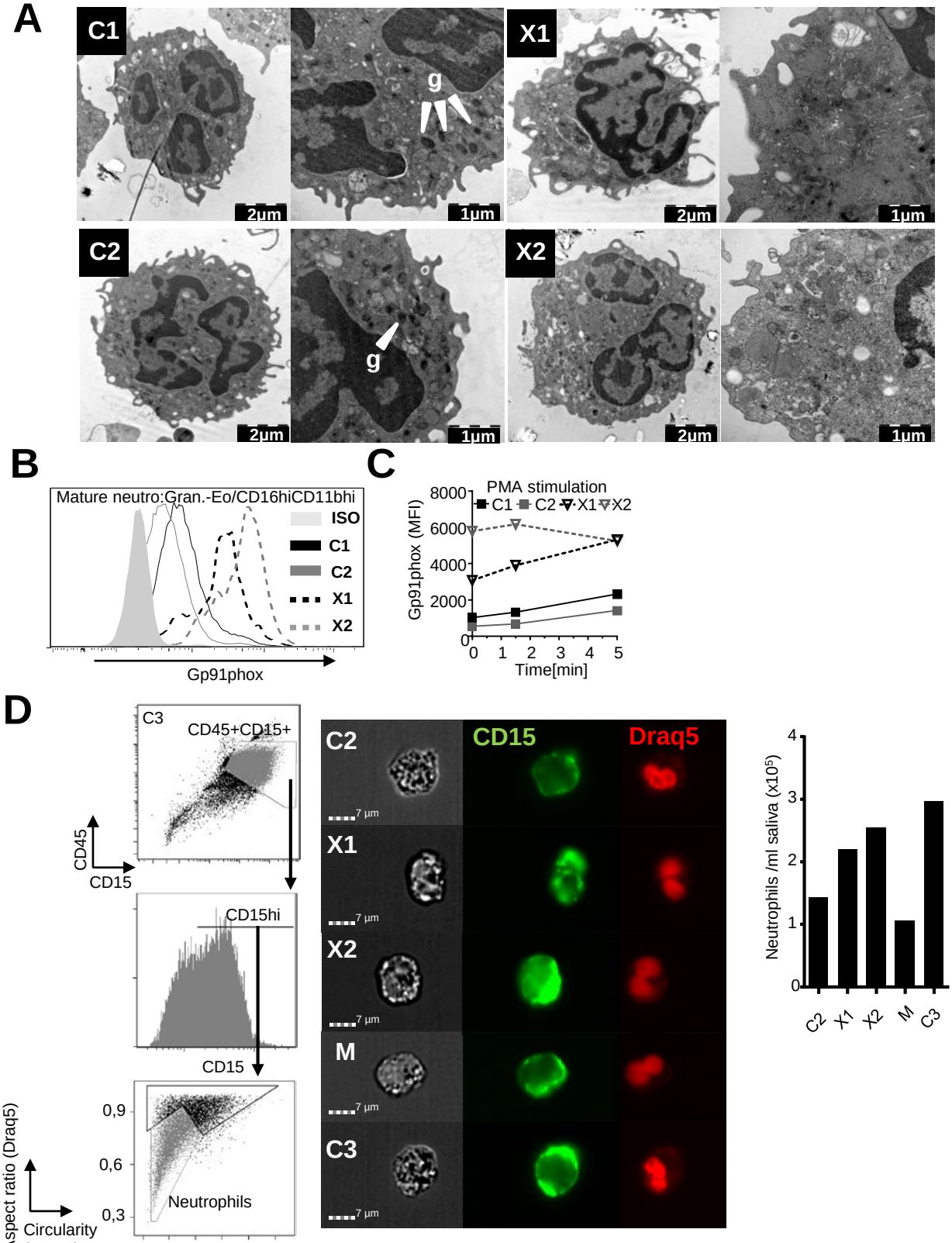
A
C1
g
2µm
1µm
X1
2µm
1µm
C2
g
2µm
1µm
X2
2µm
1µm
B
Mature neutro:Gran.-Eo/CD16hiCD11bhi
ISO
C1
C2
X1
X2
Gp91phox
C
PMA stimulation
C1 C2 X1 X2
Gp91phox (MFI)
8000
6000
4000
2000
0
0 1 2 3 4 5
Time[min]
D
C3
CD45+CD15+
CD45
CD15
CD15hi
CD15
0,9
0,6
0,3
Neutrophils
Aspect ratio (Draq5)
Circularity (Draq5)
0 10 20 30 40 50
C2
CD15
Draq5
7 µm
X1
7 µm
X2
7 µm
M
7 µm
C3
7 µm
Neutrophils /ml saliva (x10⁵)
4
3
2
1
0
C2 X1 X2 M C3

Figure 2. XLN neutrophils are hyper-activated in blood and they are at normal number in saliva.
(A) Representative transmission electron microscopy images of neutrophils from gradient purified granulocyte preparation. g: electron-dense granules. (B-C) Gp91phox expression on mature neutrophils (Granulocytes-Eosinophils/CD16HICD11bHI) from WASp L270P XLN patients (X1,X2) and two healthy male controls (C1,C2) before (B) or after (C) PMA stimulation and analyzed by flow cytometry. (D - left panel) Representative imaging flow cytometer plots of CD45 vs. CD15 staining and morphology parameters of Draq5 stained nuclei (circularity vs. aspect ratio). (D - middle panel). Example images of neutrophils ($CD45^{+}CD15^{hi}$ $Draq5[Aspect\ ratio]^{lo}$ $Draq5[Circularity]^{lo}$) taken with imaging flow cyctometer. (D - right panel) Quantitative analysis of neutrophil number/ml saliva.

Figure 3

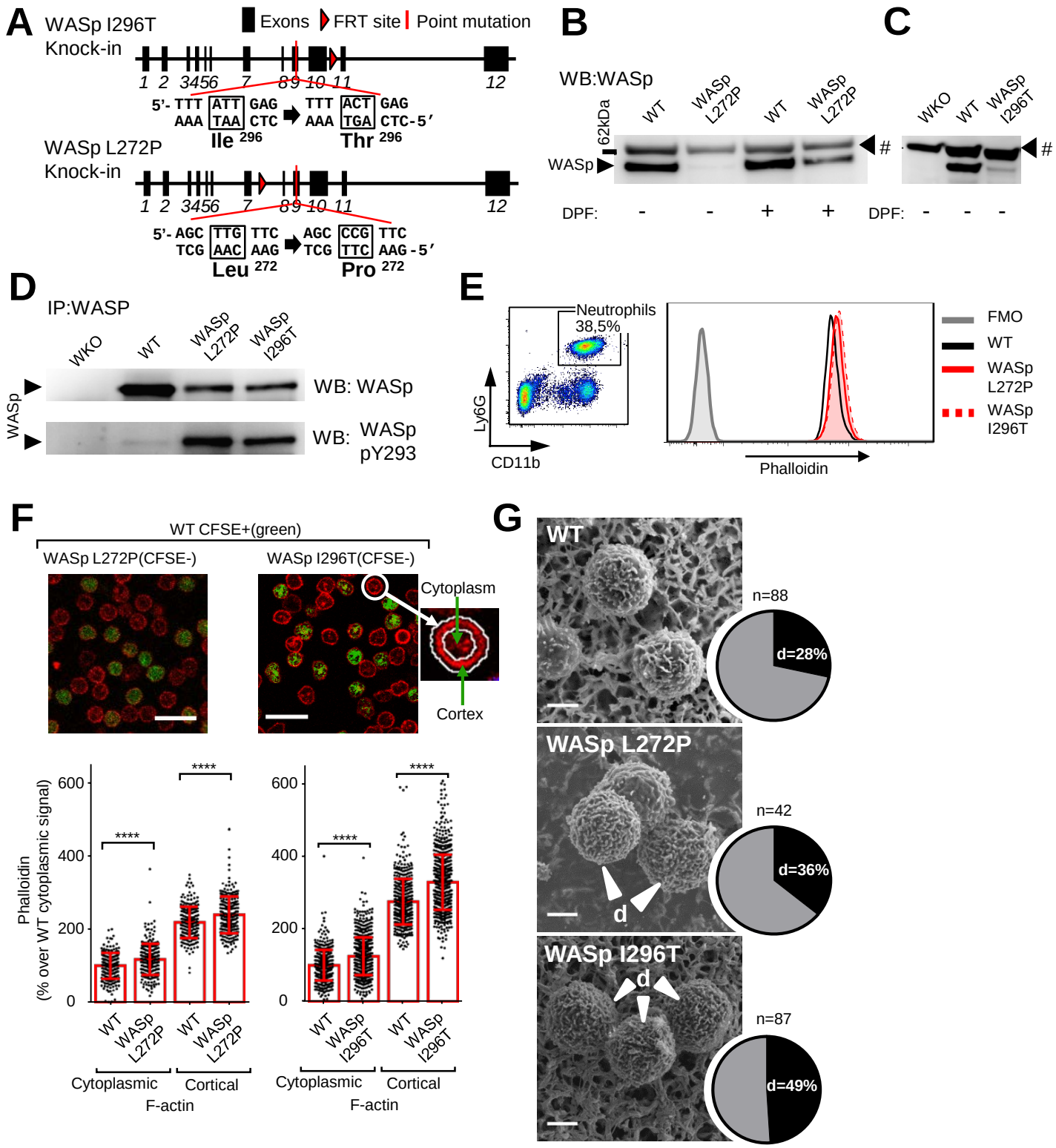
A
WASp I296T Knock-in
Exons
FRT site
Point mutation
1 2 3456 7 89 10 11 12
5'- TTT ATT GAG TTT ACT GAG
AAA TAA CTC AAA TGA CTC-5'
Ile 296
Thr 296
WASp L272P Knock-in
1 2 3456 7 89 10 11 12
5'- AGC TTG TTC AGC CCG TTC
TCG AAC AAG TCG TTC AAG-5'
Leu 272
Pro 272
B
WB:WASp
62kDa
WT
WASp L272P
WT
WASp L272P
WASp
#
DPF: - - + +
C
WKO
WT
WASp I296T
#
DPF: - - -
D
IP:WASP
WKO
WT
WASp L272P
WASp I296T
WASp
WB: WASp
WB: WASp pY293
E
Neutrophils 38,5%
Ly6G
CD11b
FMO
WT
WASp L272P
WASp I296T
Phalloidin
F
WT CFSE+(green)
WASp L272P(CFSE-)
WASp I296T(CFSE-)
Cytoplasm
Cortex
Phalloidin (% over WT cytoplasmic signal)
600
400
200
0
****
WT
WASp L272P
WT
WASp L272P
Cytoplasmic
Cortical
F-actin
WT
WASp I296T
WT
WASp I296T
Cytoplasmic
Cortical
F-actin
G
WT
n=88
d=28%
WASp L272P
n=42
d=36%
d
WASp I296T
d
n=87
d=49%

Figure 3. Increased polymerized actin, WASp Y293 phosphorylation, decreased WASp stability, and altered surface topography in mouse models of XLN. (A) Genomic organization, locations and sequences of the introduced I296T and L272P mutations in the mouse *WASp* gene. (B, C) Protein expression of WASp in lysates of WT, WASp L272P, WASp I296T, and WASp KO (WKO) peritoneal neutrophils with or without pretreatment of cells with diisopropylfluorophosphate (DPF). WASp was detected by western blotting (WB). #: unknown protein. n=3 experiments.(D) Protein expression (upper panel) and Y293 phosphorylation (lower panel) of WASp in WKO, WT, WASp L272P, and WASp I296T in immunoprecipitated protein lysates of bone marrow neutrophils. n=3 experiments.(E) FACS plot of $Ly6G^{+}CD11b^{+}$ neutrophils in mouse peripheral blood. F-actin content of neutrophils was measured with fluorescently labeled phalloidin and flow cytometry. A representative image of three individual blood samples per genotype. (F) Quantitative analysis of cortical and cytoplasmic F-actin, labelled with phalloidin (red), in bone marrow neutrophils. Outlines of cells were recognized by Fiji software and the cortex defined by a ring encompassing the outline. Integrated fluorescent intensity in the ring area and within the ring was measured and values from individual cells were plotted. CFSE labeling (for all genotypes both labelled and unlabeled samples) was used to differentiate between genotypes in each individual field. Data was normalized for the average of WT cytoplasmic signal (100%). Scale bar = 20μM. WASp I296T (n = 752) vs. WT (n = 482); WASp L272P (n = 256) vs. WT (n = 231). Mean±SD. Unpaired, 2-tailed Student's t-test. (G) Surface structure of WT, WASp L272P, and WASp I296T neutrophils. Cells were isolated from bone marrow, fixed in paraformaldehyde and photographed with scanning electron microscopy (SEM). The percentage of cells with dense surface ruffles (d) were counted manually. Scale bar = 2μM. ****: $p<0.0001$.

Figure 4

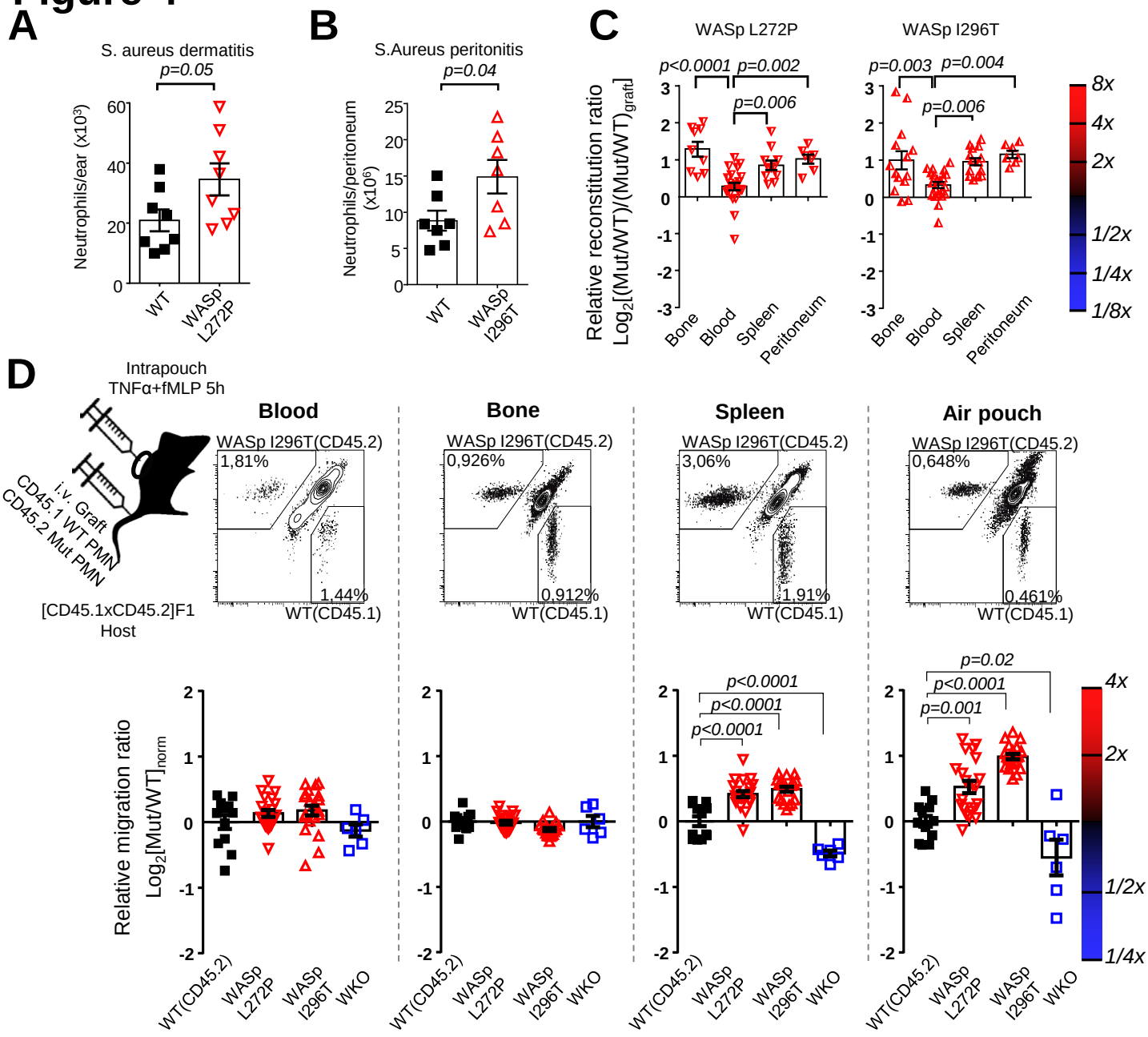

Figure 4. Increased rate of migration of WASp L272P and WASp I296T neutrophils to the spleen and to the inflammation site *in vivo*. (A) Neutrophil numbers in ears of WT and WASp L272P mice 6h after induction of dermatitis with *S. aureus* (10^6 CFU) injection. Mean±SEM. Unpaired, 2-tailed Student's t-test; WT n=8; WASp L272P n=8/group. (B) WT and WASp I296T neutrophil numbers in peritoneum 24h after injection of *S. aureus* ($20x10^6$ CFU). Mean±SEM. Unpaired, 2-tailed Student's t-test; WT n=7; WASp I296T n=7/group. (C) WASp L272P/CD45.1 WT (left panel) and WASp I296T/CD45.1 WT (right panel) neutrophil ratios in various organs in mixed bone marrow chimera mice were normalized with their original bone marrow reconstitution ratio (CD45.2/CD45.1) and plotted with logarithmic scale. Mean±SEM, One-way ANOVA with Bonferroni correction; WASp L272P/CD45.1: WT n(bone)=9; n(blood)=22; n(spleen)=11; n(peritoneum)=7; WASp I296T/CD45.1: WT n(bone)=14; n(blood)=21; n(spleen)=14; n(peritoneum)=7/group. (D) *In vivo* homing of WASp L272P (CD45.2), WASp I296T (CD45.2) and CD45.1 WT cells into various tissues was measured 5h after i.v. injection of bone marrow neutrophil grafts. Graft neutrophils (CD45.1+ or CD45.2+ single positive) were counted in blood, bone marrow, spleen, and airpouch lavage. The normalization formula is explained in materials and methods. Pool of at least 2 experiments per genotype. Mean±SEM, One-way ANOVA with Bonferroni correction; WT n=12; WASp I296T n=20; WASp L272P n=21; WKO n=6/group.

Figure 5

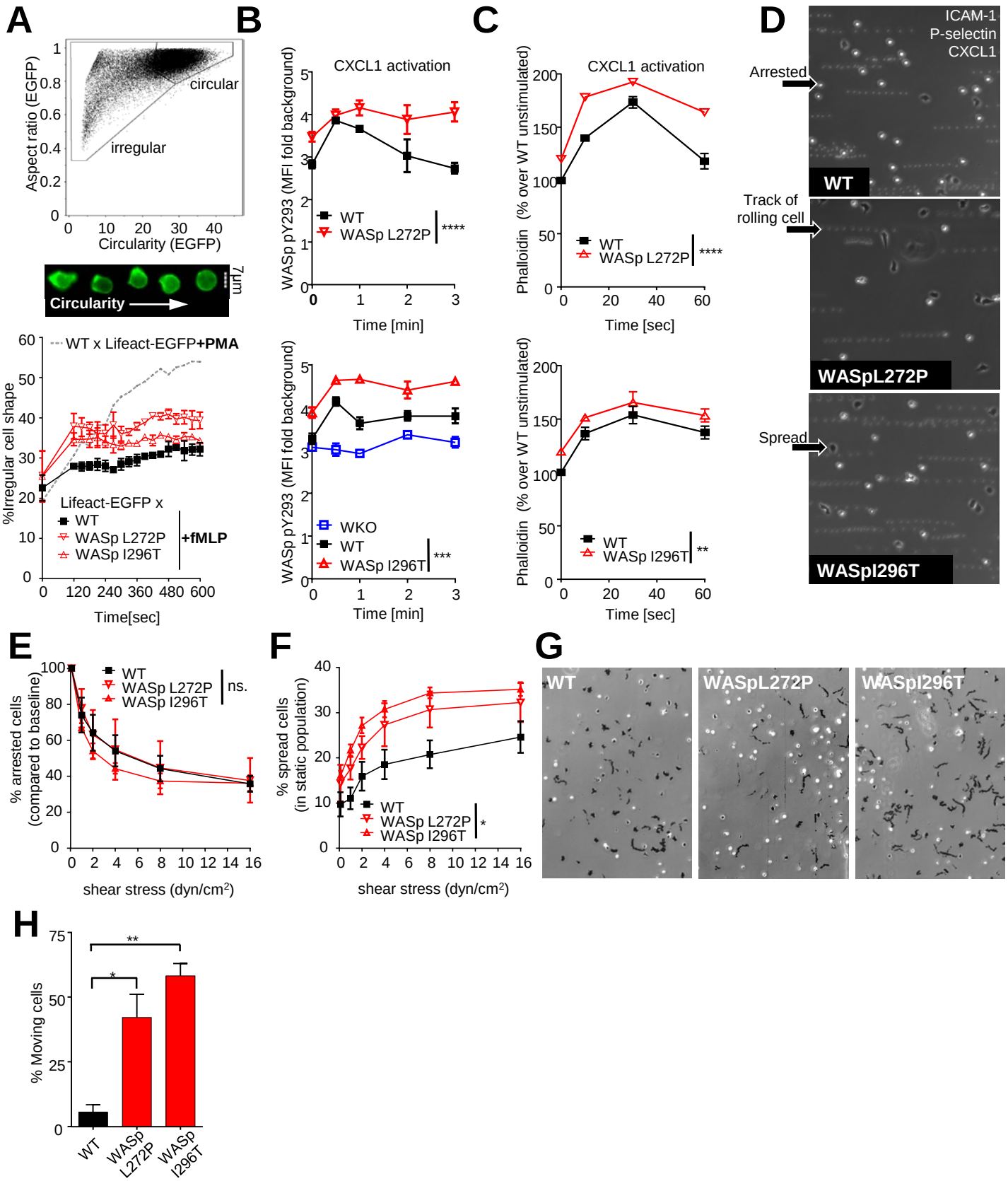
A
B
C
D
Aspect ratio (EGFP)
Circularity (EGFP)
circular
irregular
Circularity
7µm
WT x Lifeact-EGFP+PMA
%Irregular cell shape
Time[sec]
Lifeact-EGFP x
WT
WASp L272P
WASp I296T
+fMLP
CXCL1 activation
WASp pY293 (MFI fold background)
Time [min]
WT
WASp L272P
****
WKO
WASp I296T
***
Phalloidin (% over WT unstimulated)
Time [sec]
**
ICAM-1
P-selectin
CXCL1
Arrested
Track of rolling cell
Spread
WT
WASpL272P
WASpI296T
E
F
G
% arrested cells (compared to baseline)
shear stress (dyn/cm²)
ns.
% spread cells (in static population)
*
H
% Moving cells
WASp L272P
WASp I296T

Figure 5. Increased actin dynamics and spreading on ICAM-1 in WASp XLN neutrophils. (A) Live cell actin kinetics after neutrophil activation with fMLP was quantified by imaging flow cytometer. Plot of circularity and aspect ratio (upper panel) was calculated on EGFP images. Example images (middle panel) show WT x Lifeact-EGFP cells with increasing circularity. Ratio of irregular (GFP [Aspect ratio]^{lo} GFP[Circularity]^{lo}) shaped cells as the function of time (lower panel) . Kinetics was calculated after binning data to 30 sec timeframes. >15000 cells / each genotype; 2 independent experiments per genotype. (B) Kinetics of WASp Y293 phosphorylation upon CXCL1 treatment was quantified with imaging flow cytometer after intracellular staining of phospho-Y293 WASp. Phospho-Y293 WASp signal was depicted as fold change of pY293 integrated intensity over background (secondary antibody staining only). n=3, n=4 experiments. (C) Kinetics of F-actin polymerisation upon CXCL1 treatment was quantified with phalloidin staining and flow cytometer. n=3, n=3 experiments. (D) rmP-selectin, rmICAM-1, and rmCXCL-1 coated plastic flow chambers were perfused with bone marrow neutrophils at 0,1 dyn/cm^2. Representative images were taken after increasing flow rate to 2 dyn/cm^2. Motility was assessed by overlaying 10 consecutive frames. (E) Number of arrested cells were counted and depicted as % of arrested cells at 0,1 dyn/cm^2 after increasing flow rate stepwise with 30 sec of run at each indicated sheer stress. n=3, n=3 experiments. (F) Ratio of spread cells at increasing flow rate. (G) Neutrophils in rmP-selectin, rmICAM-1, and rmCXCL-1 coated plastic flow chambers at 2 dyn/cm^2 shear stress. Black tracks indicate the motility of adherent cells within a 20 minute time period. n=3 images/genotype.

Data is represented as mean±SEM. One-way or two-way ANOVA was used and Bonferroni multiple comparison test for statistical significance. *: $p<0.05$, **: $p<0.01$, ***: $p<0.001$, ****: $p<0.0001$.

Figure 6

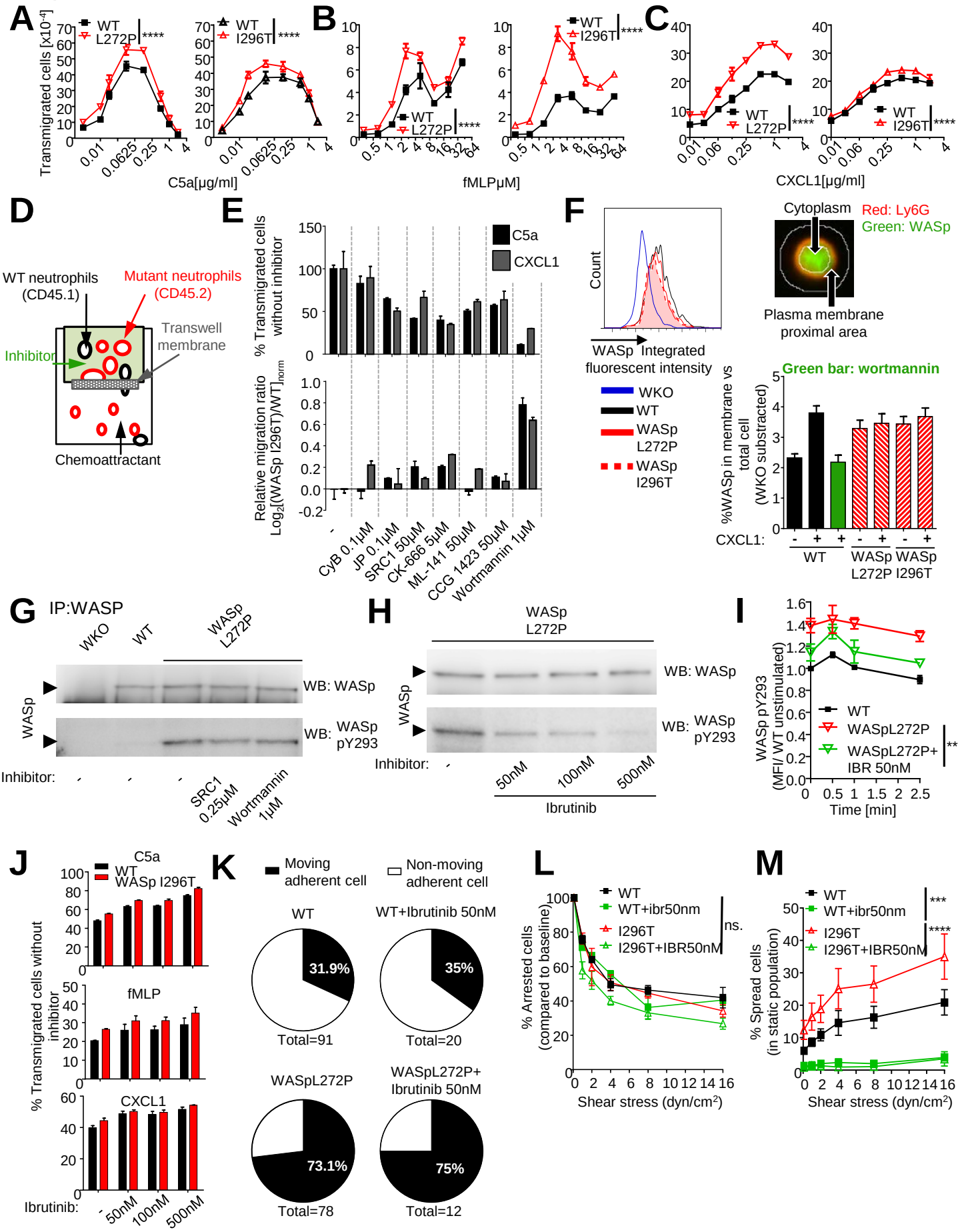
A
B
C
WT
L272P
I296T
****
Transmigrated cells [x10^-4]
C5a[µg/ml]
fMLPµM]
CXCL1[µg/ml]
D
WT neutrophils (CD45.1)
Mutant neutrophils (CD45.2)
Transwell membrane
Inhibitor
Chemoattractant
E
% Transmigrated cells without inhibitor
C5a
CXCL1
Relative migration ratio Log2(WASp I296T)/WT)norm
CyB 0.1µM
JP 0.1µM
SRC1 50µM
CK-666 5µM
ML-141 50µM
CCG 1423 50µM
Wortmannin 1µM
F
Count
WASp Integrated fluorescent intensity
WKO
WT
WASp L272P
WASp I296T
Cytoplasm
Red: Ly6G
Green: WASp
Plasma membrane proximal area
Green bar: wortmannin
%WASp in membrane vs total cell (WKO substracted)
CXCL1:
WT
WASp L272P
WASp I296T
G
IP:WASP
WKO
WT
WASp L272P
WASp
WB: WASp
WB: WASp pY293
Inhibitor:
SRC1 0.25µM
Wortmannin 1µM
H
WASp L272P
WASp
WB: WASp
WB: WASp pY293
Inhibitor:
50nM
100nM
500nM
Ibrutinib
I
WASp pY293 (MFI/ WT unstimulated)
WT
WASpL272P
WASpL272P+ IBR 50nM
Time [min]
J
C5a
WT
WASp I296T
fMLP
CXCL1
% Transmigrated cells without inhibitor
Ibrutinib:
50nM
100nM
500nM
K
Moving adherent cell
Non-moving adherent cell
WT
WT+Ibrutinib 50nM
31.9%
35%
Total=91
Total=20
WASpL272P
WASpL272P+ Ibrutinib 50nM
73.1%
75%
Total=78
Total=12
L
WT
WT+ibr50nm
I296T
I296T+IBR50nM
ns.
% Arrested cells (compared to baseline)
Shear stress (dyn/cm2)
M
WT
WT+ibr50nm
I296T
I296T+IBR50nM
***
****
% Spread cells (in static population)
Shear stress (dyn/cm2)

Figure 6. Increased *in vitro* migration, membrane translocation and Btk dependent phosphorylation of WASp in XLN neutrophils. (A, B, C) Migration of WT vs. WASp L272P (left panel) and WASp I296T (right panel) bone marrow neutrophils towards different concentrations of C5a, CXCL1, fMLP in transwell plates. Transmigrated cell numbers were measured by flow cytometry. n=3, n=3 experiments/chemoattractant. (D, E) WT (CD45.1) and WASp XLN (CD45.2) neutrophils were mixed 1:1 ratio in the upper well of a transwell plate and incubated for 10 min with various inhibitors. Migration rate towards C5a or CXCL1 was quantitated with flow cytometry. n=2 experiments. (F) WASp intracellular expression was measured by imaging flow cytometer. WASp intracellular distribution was assessed by calculating ratios of plasma membrane proximal (determined by Ly6G surface staining) WASp and WASp in the total cell in flow cytometer images. Mean+SEM of at least 198 neutrophils. n=3 experiments. (G) WASp and phospho-Y293 WASp proteins in SRC1 and Wortmannin pretreated neutrophils were measured by Western blot. n=2. (H) WASp and phospho-Y293 WASp in WASp L272P neutrophils before and after Ibrutinib treatment. n=3. (I) WASp Y293 phosphorylation upon CXCL1 activation with or without Ibrutinib treatment measured with flow cytometry. n=3. (J) Transwell migration of WT and WASp I296T neutrophils towards C5a (0.125µg/ml), fMLP (3µM), and CXCL1 (0.25 µg/ml) after incubation with the indicated concentrations of Ibrutinib. n=3. (K) Ratio of motile cells among adherent cells on rmP-selectin, rmICAM-1, and rmCXCL-1 under flow as on Figure 5G. (L) Number of arrested cells were counted and depicted as % of arrested cells at 0,1 dyn/cm^2 as on Figure 5E. (M) Ratio of spread cells at increasing flow rate as on Figure 5F. n=3, n=2 experiments. Data is represented as mean±SEM. One-way or two-way ANOVA was used for statistical significance. *: p<0.05, **: p<0.01, ***: p<0.001, ****: p<0.0001.

Figure 7

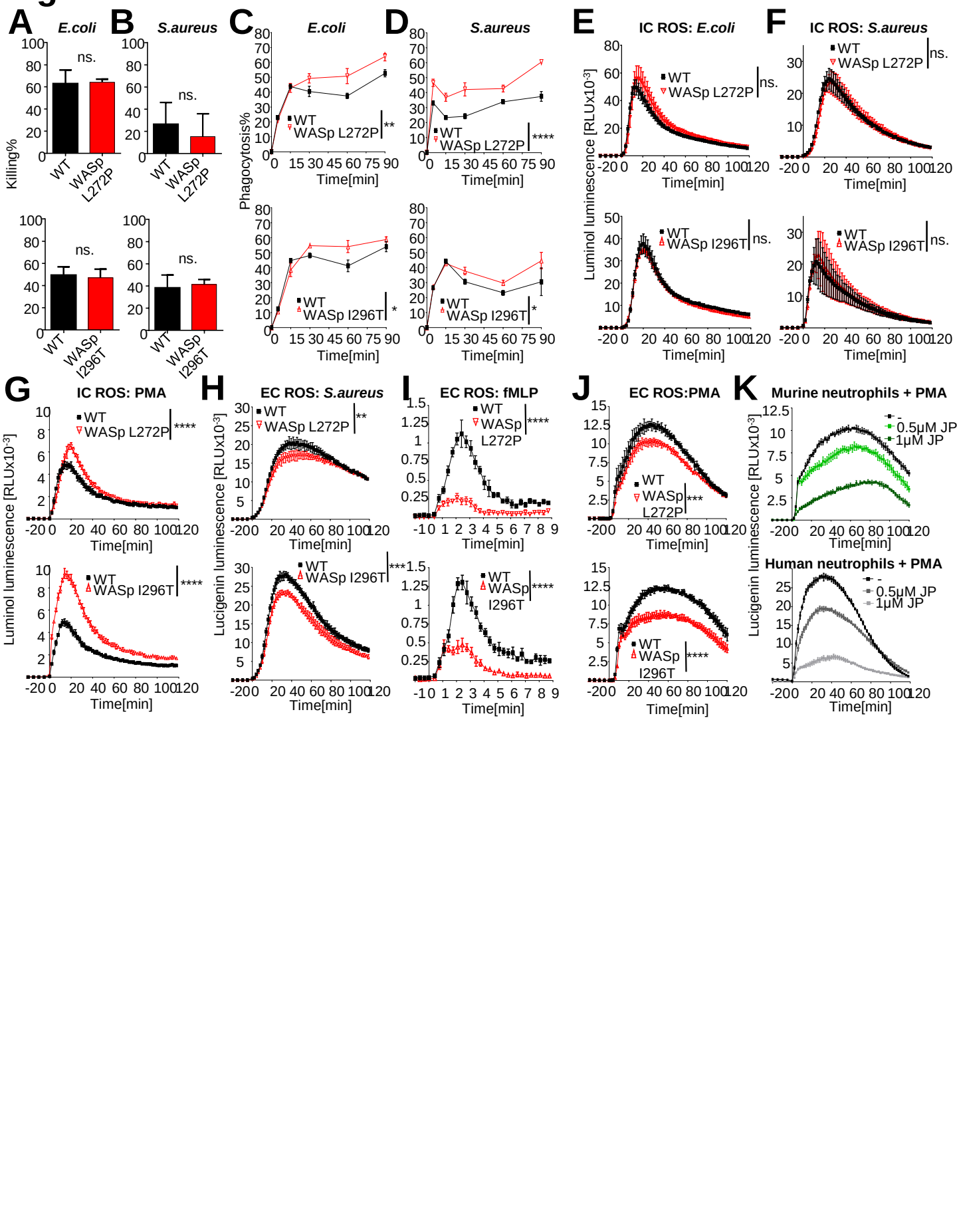
A
E.coli
B
S.aureus
Killing%
ns.
WT
WASp L272P
WASp I296T
C
E.coli
D
S.aureus
Phagocytosis%
WT
WASp L272P
WASp I296T
**
****
*
Time[min]
E
IC ROS: E.coli
F
IC ROS: S.aureus
Luminol luminescence [RLUx10-3]
Lucigenin luminescence [RLUx10-3]
***
G
IC ROS: PMA
H
EC ROS: S.aureus
I
EC ROS: fMLP
J
EC ROS:PMA
K
Murine neutrophils + PMA
Human neutrophils + PMA
0.5μM JP
1μM JP

Figure 7. Increased phagocytosis rate, normal killing of bacteria and dysregulated ROS responses in XLN neutrophils. *E.coli* (A) or *S.aureus* (B) killing capacity of WT and WASp XLN neutrophils was assessed by co-incubating serum opsonized bacteria and neutrophils at a ratio of 1:5 (*E.coli* : neutrophil) for 60 minutes (A) or 1:1 (*S.aureus* : neutrophil) for 60 and 90 minutes in upper and lower panel respectively (B). n=3, n=3 experiments with each bacteria. (C, D) Phagocytosis of Alexa488 labelled serum opsonized *E. coli* (C) and *S. aureus* (D) by WT WASp XLN neutrophils measured by flow cytometry. n=3, n=3 experiments with each bacteria. (E, F, G) Intracellular ROS (IC ROS) measured with luminol chemiluminescence in murine bone marrow neutrophils upon stimulation with E.coli (n=8) (E), *S.aureus* (n=10) (F), or PMA (n=18). n=4, Mean±SD, Two-way ANOVA. (H, I, J) Extracellular ROS (EC ROS) was measured using a lucigenin chemiluminescence assay in murine bone marrow neutrophils upon stimulation with (H) heat-killed serum opsonized *S. aureus* (n=18), (I) fMLP (n=4), or (J) PMA (n=26). n=4, Mean±SD, Two-way ANOVA. (K) Extracellular ROS was measured upon PMA stimulation of murine (upper panel) and human healthy donor (lower panel) neutrophils with or without pre-treatment with jasplakinolide. n=5, Mean±SD .*: $p<0.05$, **: $p<0.01$, ***: $p<0.001$, ****: $p<0.0001$.

Figure 8

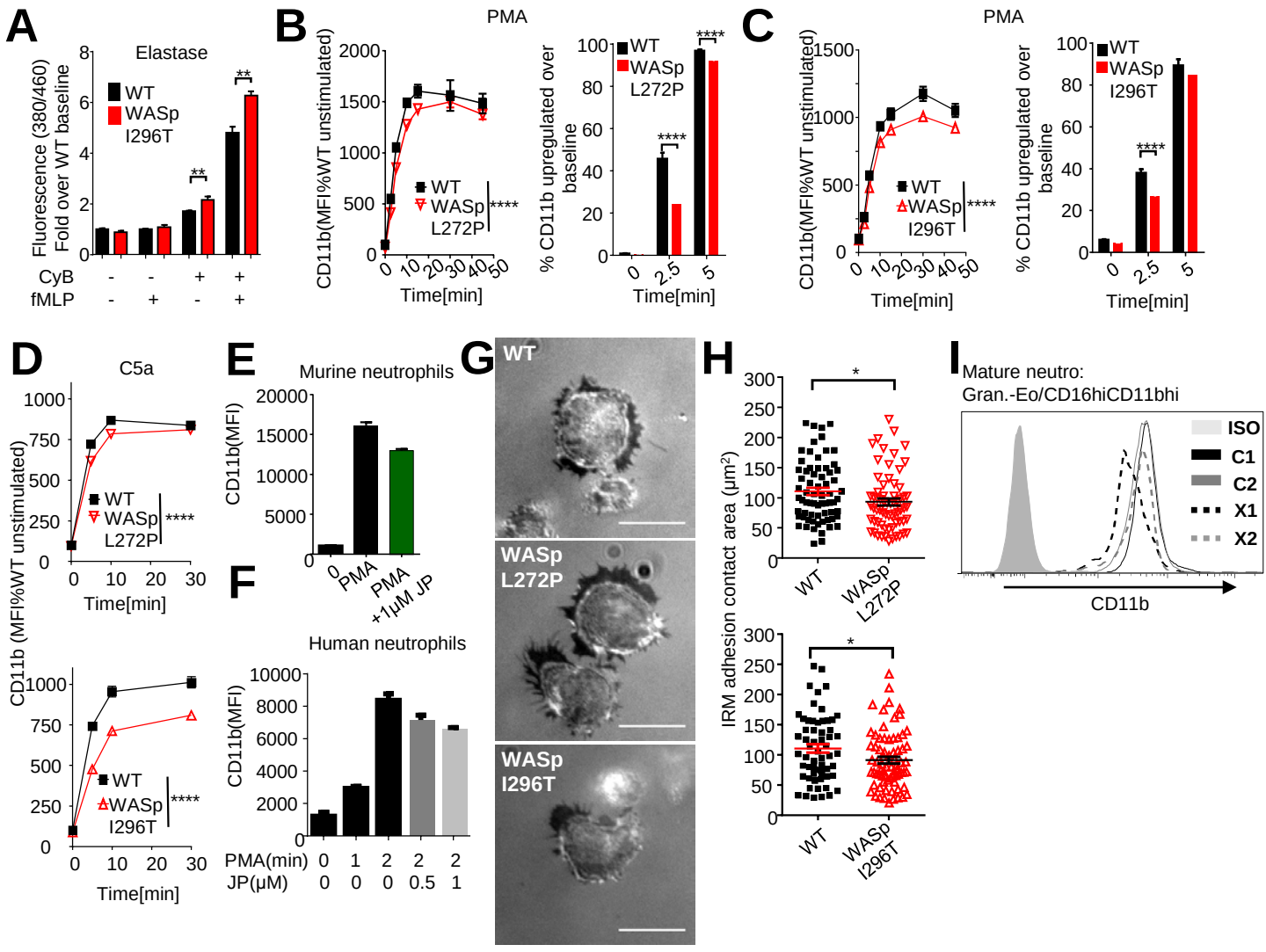

Figure 8. Altered granule release in XLN neutrophils. (A) Neutrophil elastase secretion by WT and WASp I296T neutrophils was measured with fluorescent detection of the cleavage of MeOSuc-AAPV-AMC substrate after 90 min activation with 10 µM fMLP in the presence of 5µg/ml Cytochalasin B (CyB). n=4, n=3 experiments. (B, C) Upregulation of CD11b upon activation of bone marrow derived neutrophils with PMA (left panel) . Data is represented as percentage of WT unstimulated signal. Percentage of cells above arbitrary baseline MFI of CD11b (right panel) . Bonferroni corrected t-test. n=4, n=4 experiments. (D) CD11b expression of bone marrow derived neutrophils upon C5a stimulation. Two-way ANOVA. n=3. (E, F) CD11b expression on PMA activated murine (E) and human (F) neutrophils. When indicated, neutrophils were pre-incubated 30 min with jasplakinolide. Murine: n=3; human: n=2. (G) Interference reflection microscopy (IRM) images of 5 minutes fMLP activated, adherent neutrophils on fibrinogen coated glass. Scale bar: 10µm. (H) Quantification of adhesion contact area on IRM images. Minimum count of 14 fields per genotype, Mann-Whitney test. n=4 experiments. (I) CD11b expression on mature neutrophils (Granulocytes-Eosinophils/CD16HICD11bHI) from WASp L270P XLN patients (X1,X2) and two healthy male controls (C1,C2) analyzed by flow cytometry. Unless otherwise indicated , data is represented as mean±SEM. One-way or two-way ANOVA was used to test statistical significance. *: p<0.05, **: p<0.01, ***: p<0.001, ****: p<0.0001.